J. Fluid Mech. (2004), *vol.* 503, *pp.* 171–200.
DOI: 10.1017/S0022112003007699 Printed in the United Kingdom

Weakly nonlinear analysis of wind-driven gravity waves

By ALEXANDROS ALEXAKIS[1], YUAN-NAN YOUNG[2] AND ROBERT ROSNER[1,3]

[1]Department of Physics, University of Chicago, Chicago, IL 60637, USA
[2]Department of Engineering Sciences & Applied Mathematics, Northwestern University, Evanston, IL, 60208, USA
[3]Department of Astronomy & Astrophysics, University of Chicago, Chicago, IL 60637, USA

(Received 6 January 2003 and in revised form 3 October 2003)

We study the weakly nonlinear development of shear-driven gravity waves induced by the physical mechanism first proposed by Miles, and furthermore investigate the mixing properties of the finite-amplitude solutions. Linear theory predicts that gravity waves are amplified by an influx of energy through the critical layer, where the velocity of the wind equals the wave phase velocity. As the wave becomes of finite amplitude nonlinearities have to be taken into account. In this paper we derive asymptotic solutions of finite-amplitude waves for weak wind and strong gravitation $U^2 \ll gl$, applicable to many astrophysical scenarios. Because of the presence of a critical layer, ordinary weakly nonlinear methods fail; in this paper, we use rescaling at the critical layer and matched asymptotics to derive the amplitude equations for the most unstable wave, under the assumption that the physical domain is periodic. These amplitude equations are compared with the equations derived by Reutov for the small-density-ratio case (applicable to oceanography); and after numerically integrating these equations, we also analytically derive their quasi-steady limit. As in other analyses of critical layers in inviscid parallel flow, we find that the initial exponential growth of the amplitude A transitions to an algebraic growth proportional to the viscosity, $A \sim \nu t^{2/3}$. We also find that the weakly nonlinear flow allows superdiffusive particle transport within the critical layer, with an exponent $\sim 3/2$, consistent with Venkataramani's results.

1. Introduction

The generation of surface waves by wind has been a problem under study for well over a century. Lord Kelvin and Helmholtz (KH) investigated the stability of fluid interfaces using a simple model of a step function wind shear profile. However, they found higher bounds on the maximum wind velocity for the instability to occur than field measurements (Chandrasekhar 1961, § 101). This discrepancy was not resolved until Miles (1957, 1959*a*,*b*, 1962, 1967) proposed a model in which gravity waves are amplified through a 'resonant' interaction with the wind above the ocean surface. Assuming a turbulent boundary-layer wind profile of the form $\log(y/y^*)$ (where y is the height above sea level and y^* is the stiffness parameter), Miles found that waves with phase speed $c = \sqrt{g/k}$ are amplified through resonance with the the wind at height y_c, where the wind velocity $U(y)$ matches the wave speed, $U(y = y_c) = c$ (g and

k are, as is customary, the gravitational acceleration and wavenumber, respectively). At this critical layer, where the wind velocity equals the phase speed of the gravity wave, the solution to the linear eigenvalue problem becomes singular as the x-component of the perturbation velocity behaves as $u \sim \log(y - y_c)$. The singularity is removed either because there is an imaginary component of c (i.e. unsteady critical layer) or because viscosity becomes important in this thin layer (i.e. viscous critical layer). In both cases, the final result is that there is an '$-i\pi$ phase change' across the critical layer such that the perturbation wave above the critical layer is not in phase with the wave below. A direct result of this phase change is that the gravity wave will become unstable because a component of the pressure perturbation will be in phase with the slope of the wave (unlike the KH case, in which the pressure perturbation wave is always in phase with the crest of the wave). Using the results from linear theory and for small density ratios, Miles estimated the energy flux from the wind to the gravity wave.

Our interest in this problem is motivated by an astrophysical puzzle, namely, the mixing of carbon/oxygen (C/O) at the surface of a white dwarf with accreted material (mostly hydrogen and helium, He/H) overlying the stellar surface (whose presumed origin is from an accretion disk surrounding the compact star). For a variety of reasons, it is thought that the accreted envelope is in differential rotation with respect to the stellar surface, so that a 'wind' is expected at this surface (Rosner *et al.* 2001). In this stellar case, one has to generalize the earlier results to arbitrary density ratios (between the 'atmosphere' and the 'surface material'). We have already done so for the linear problem (Alexakis, Young & Rosner 2002), deriving bounds on the instability in the parameter space, and estimating the growth rates of the unstable modes. However, linear theory gives no information about the ultimate fate of the system, which is governed largely by nonlinear processes.

In this paper, we uncover the nonlinear evolution of wind-driven surface waves by examining their finite-amplitude evolution using an asymptotic expansion. There are a number of alternative ways to study the nonlinear behaviour of wind-driven surface waves, such as for example turbulent modelling of the wind–wave coupling (Harris, Belcher & Street 1996; Belcher, Harris & Street 1994; Jenkins 1992); our focus is instead on weakly nonlinear theory because we seek a first-principles understanding of the effects of nonlinearities as the wave amplitude emerges from the linear regime. We further note here that the weakly nonlinear theory for the KH instability has already been derived by Drazin (1970); and that a Ginzburg–Landau equation was also derived for viscous flow by Blennerhassett (1980) and Akylas (1982) for cases where viscous dissipation dominates in saturating the gravity wave amplitude. However, classical finite-amplitude analysis in the weakly nonlinear limit cannot be applied straightforwardly to our problem because of the presence of critical layers: due to the singularity that appear in the linear theory at the point where the phase speed of a surface wave matches the wind speed, higher-order terms in the expansion become more singular and the expansion must ultimately fail. The fundamental reason for this behaviour is that the flow becomes nonlinear first inside the critical layer, even though the rest of the flow can still be considered as operating in the linear regime. For this reason, a more refined treatment of the critical layer is required. The necessary analytical 'machinery' fortunately already exists: thus, Benney & Bergeron Jr. (1969), and later Benney & Maslowe (1975), showed that for small but finite amplitudes the phase change at the critical layer does not necessarily have to be $-i\pi$; instead, they found that the phase change is zero if the nonlinear terms are taken into account. Later Haberman (1972) showed numerically that there is a

smooth increase of the phase change, from $-i\pi$ to 0, and introduced the function Φ_H that gives the phase change as a function of the amplitude; Churilov & Shukhman (1987, 1996) and Shukhman & Churilov (1997) then derived an ordinary differential equation to describe the evolution of the amplitude of the perturbation based on Φ_H and other similar functions defined for the appropriate critical layer problem. A fundamental assumption in all this work is that the viscosity is dominant in the critical layer; this leads to the derivation of an ordinary differential equation for the wave amplitude. The full equations of the weakly nonlinear problem without the previous assumption have then been derived and solved numerically for various cases (Goldstein & Hultgren 1988; Warn & Warn 1978; Balmforth & Piccolo 2001).

In our case the treatment – although closely related to the earlier work – is nevertheless different in some respects. The previously discussed cases were dealing with a smooth neutral mode where the critical layer was formed at the inflection point $\mathrm{d}^2U/\mathrm{d}y^2 = 0$. The problem at hand though, deals with neutral modes (gravity waves) that are weakly coupled to a non-modal disturbance in the critical layer in the upper layer. Unlike the previous cases the marginally unstable modes do not form a critical layer at the inflection point since such an inflection point does not exist. Instead gravity waves become weakly unstable if the coupling between the upper fluid (wind) and the gravity modes of the lower fluid is weak. This can be the result of a small coupling coefficient (small density ratio) or if the wind velocity is close to but higher than the smallest phase velocity of the gravity waves. This allows us to examine two special cases: small density ratio, and weak wind or strong stratification; in both cases, the linear growth rate is small. The first case has been examined by Reutov (1980) and applied to ocean waves. We will focus on the second case, which is of particular interest to our astrophysical problem, since the instability takes place on the surface of a white dwarf star, i.e. a star of solar mass, but comparable in size to the Earth; this corresponds to the strongly stratified limit. Another technical difference from the previous cases appears in the derivation of the amplitude equations and lies in the fact that we have a sharp interface. Because of this, our solvability condition will not be expressed in terms of integrals but rather in terms of appropriate vector products of the values of the perturbation stream function at the interface.

An interesting aspect we further examine, with direct applications to the relevant astrophysical and geophysical systems, is the mixing properties of the finite-amplitude equations. Although the weakly nonlinear results do not lead to wave breaking, which is the main mechanism for mixing the 'surface material' with the 'atmosphere', we study the mixing of tracers inside the critical layer as a first step to revealing the mixing properties of the fully nonlinear problem. We measure the finite-time Lyapunov exponents and the particle dispersion of the flow.

This paper is structured as follows. First we formulate our problem and describe the non-dimensionalized form of the basic problem equations. In § 3 we briefly review the linear theory developed earlier (Alexakis *et al.* 2002). The amplitude equations are derived in § 4 for the strongly stratified case and generalize the results of Reutov (1980). We summarize the conservation laws from the amplitude equations in § 5.1, and we discuss the implications of the long-time behaviour of surface waves in § 5.2. In § 5.3 we present the results from numerically simulating the amplitude equations. In § 6 we investigate how the coupling between the wind and the surface wave affects mixing properties of the finite-amplitude solution. A detailed examination of the assumptions made in the analysis is provided in § 7, where we also draw conclusions from our work.

2. Formulation

We consider a two-layer system with constant fluid density ρ_1 and ρ_2 ($\rho_1 \leqslant \rho_2$) in the upper and lower layers, respectively. The interface between the two layers is given by $y = h(x, t)$, where x is the horizontal and y is the vertical coordinate. In the upper layer we assume a wind parallel to the originally flat interface $y = h(x, t = 0) = 0$. The wind has a shear velocity profile $\boldsymbol{U} \equiv [U(y), 0]$, where $U(y)$ varies only with y. The lower layer is initially at rest; thus, we will not consider the more complex, albeit more realistic, case of additional shear in the lower layer (Caponi *et al.* 1992). Our aim is to study the dynamics and the weakly nonlinear development of small sinusoidal perturbations of the horizontal interface.†

The fluid is assumed incompressible in both layers; we therefore work with the stream function Ψ, which is connected to the velocity by the relation $(u, v) = (\partial_y \Psi, -\partial_x \Psi)$. The stream function can be separated into its mean and its perturbation components,

$$\Psi_{\text{total}} = \int_0^y U \, \mathrm{d}y' + \Psi. \tag{2.1}$$

The fluid within each layer is described by the Navier–Stokes equations (in terms of the stream function Ψ):

$$\nabla^2 \Psi_{,t} + U \nabla^2 \Psi_{,x} - U_{,yy} \Psi_{,x} = \Psi_{,x} \nabla^2 \Psi_{,y} - \Psi_{,y} \nabla^2 \Psi_{,x} + \nu \nabla^2 \nabla^2 \Psi, \tag{2.2}$$

where ∇^2 is the two-dimensional Laplacian and ν is the viscosity (which we will consider to be small, and therefore negligible except for a narrow region within the critical layer). Here we have used the standard notational device of comma-prefaced subscripts to denote partial derivatives, e.g.

$$f_{,x} \equiv \partial f / \partial x.$$

The boundary conditions at the interface are the continuity of the component of the velocity perpendicular to the interface

$$h_{,t} + (U^{\pm} + \Psi^{\pm}_{,y}) h_{,x} + \Psi^{\pm}_{,x} = 0, \tag{2.3}$$

and the continuity of pressure

$$\Delta[\rho_i \{\Psi_{,ty} + (U + \Psi_{,y}) \Psi_{,xy} - \Psi_{,x}(U_{,y} + \Psi_{,yy}) - h_{,x}(\Psi_{,tx} + (U + \Psi_{,y}) \Psi_{,xx} + \Psi_{,x} \Psi_{,xy})\}] = g h_{,x} (\rho_2 - \rho_1), \tag{2.4}$$

† As an aside, we note that the presence of a sharp interface boundary between the two fluids in our system is really only a device to simplify the analysis, but in no way restricts our results. That is, in a more general case there will be no sharp interface, but the density will change smoothly from ρ_2 to ρ_1 in a layer of width δ_1. We would then also expect $U(y)$ to be a smooth function in y, so that any flow discontinuity at the interface would be replaced by a smooth variation in U within a thin viscous boundary layer of width δ_2. One would then expect to see differences in behaviour only for those modes with horizontal wavenumber k large enough so that the critical layer lies inside these layers δ_1, δ_2. Such modes, however, are KH-modes which are not under study here; they will obey a Richardson-type stability criterion, $1/4 < g \Delta\rho \delta_2^2 / [\rho (\Delta U)^2 \delta_1]$ (Chandrasekhar 1961). We therefore expect our assumption of a sharp interface to be reasonable for horizontal wavenumbers $k^{-1} \geqslant \max\{\delta_1, \delta_2\}$. Since we are primarily interested in long-wavelength perturbations, we conclude that, for our purposes, we have not disregarded any important physics.

where $h(x,t)$ is the elevation of the interface and all quantities above are evaluated at $y=h(x,t)$. The $\pm$ indices indicate values above and below the interface, and $\Delta[\,]$ denotes the difference across $y=h$ (e.g. $\Delta[f(y)]=f(h^+)-f(h^-)$).

We non-dimensionalize lengths by the characteristic length l of the wind (a typical length over which the wind strength changes), and the velocities by the asymptotic value of the wind at $y\to+\infty$, U_{max}. An important parameter that emerges from the scaling is $G\equiv gl/U_{max}^2$, which is a measure of the ratio of potential energy to kinetic energy, or alternatively, a measure of the strength of the stratification. Other dimensionless parameters are the Reynolds number, $Re\equiv U_{max}l/\nu\gg 1$, and the ratio of densities, $r\equiv\rho_1/\rho_2\leqslant 1$. In terms of the non-dimensional parameters, we focus on the case where $Re\gg 1$ in each layer, and especially the limit $G\gg 1$ (accretion on white dwarfs in astrophysics).

3. Linear theory

We linearize equations (2.2)–(2.4), and write the stream function perturbation Ψ and surface elevation h as a travelling wave parallel to the wind (right travelling wave in our setup)

$$\begin{aligned}\Psi^{\pm}(y,x,t) &= \phi^{\pm}(y)\mathrm{e}^{\mathrm{i}K(x-Ct)}+\text{c.c.},\\ h &= \tilde{h}\mathrm{e}^{\mathrm{i}K(x-Ct)}+\text{c.c.},\end{aligned}$$

where c.c. denotes the complex conjugate, $K=kl$ is the non-dimensional (horizontal) wavenumber and C is the non-dimensional phase velocity. This leads us to the well-studied Rayleigh equation (Drazin & Reid 1981)

$$\phi^{\pm}_{,yy}-\left[K^2+\frac{U_{,yy}}{U-C}\right]\phi^{\pm}=0, \tag{3.1}$$

where the inviscid limit $Re\to\infty$ is taken. The boundary conditions become

$$(U^{\pm}-C)\tilde{h}+\phi^{\pm}=0, \tag{3.2}$$

$$\Delta[\rho_i((U^{\pm}-C)\phi^{\pm}_{,y}-U^{\pm}_{,y}\phi^{\pm})]-G\tilde{h}(\rho_2-\rho_1)=0. \tag{3.3}$$

Eliminating ϕ^- and $\tilde{h}$ from the last two equations we obtain

$$KC^2-r[(U^{\pm}-C)^2\phi^{+}_{,y}-(U^{\pm}-C)U_{,y}]-G(1-r)=0, \tag{3.4}$$

where we have used $\phi^+|_{y=0}=1$ as a normalization condition.

To further simplify we assume that $U^+(0)=0$ (e.g. U is continuous) and omit the KH-modes (of which the nonlinear evolution is not under study here, see Alexakis *et al.* (2002) for more details). The linear growth rate ($K\,\mathrm{Im}(C)$) has been numerically calculated and summarized in Alexakis, Young & Rosner (2002) for cases of interests. Here we briefly summarize some relevant results on stability boundaries for the wind profile (in dimensional units $U(y)=U_{max}(1-\mathrm{e}^{-y/l})$):

$$U(y)=1-\mathrm{e}^{-y}. \tag{3.5}$$

As shown in Alexakis *et al.* (2002), this wind profile allows an analytic expression for the stability boundaries in the stability diagram. One can show that some general features of the stability boundaries summarized here for the wind profile in equation (3.5) also hold for other bounded wind profiles. The stability bound comes from the modes that have phase velocity $C=1$, in which case the solution of equation (3.1)

becomes $\phi = \mathrm{e}^{-\kappa y}$ with $\kappa = \sqrt{1+K^2}$. Applying the boundary conditions, one obtains the criterion on wavenumber K for the unstable modes:

$$K \geqslant K_{min} = \frac{G(1-r)+r-r\sqrt{(G(1-r)+r)^2+(1-r^2)}}{1-r^2}. \tag{3.6}$$

The unstable modes can be further restricted if we assume the presence of surface tension or magnetic fields. This will lead to an additional term $\mathscr{T}K^2$ in equation (3.4), where $\mathscr{T} = \sigma/(\rho_2 U_{max}^2 l)$ and σ is the surface tension‡. Then the unstable modes lie in the region $K_{min} \leqslant K \leqslant K_{max}$, where K_{min} and K_{max} are given by the positive real solutions of

$$K + r\sqrt{1+K^2} - (G(1-r)+r+\mathscr{T}(K)K^2) = 0. \tag{3.7}$$

Furthermore, there is a value of $\mathscr{T}$ below which the above equation has no positive real solutions, and therefore no unstable modes exist. The physics behind these bounds is simple: in order for a mode to become unstable for the above wind profile, the phase velocity of the wave must lie in the range $0 < c < U_{max}$ (Alexakis *et al.* 2002). With the inclusion of surface tension, the phase velocity is not monotonically decreasing with K but, rather, increases without bound for large K. This leaves only a finite region in K-space with phase velocity smaller than U_{max}; moreover, if the surface tension is large enough, the minimum phase velocity is larger than U_{max}, and therefore no unstable mode exists. For large $G \gg 1$, we must have $4\mathscr{T}G \leqslant (r+1)^2/(1-r)$ for instability from equation (3.7). In the limit $r \to 0$ the condition for instability becomes $\mathscr{T}G \leqslant 1/4$ to zeroth order in r.

The analysis is simplified if we assume small density ratio $r \ll 1$, and expand all quantities in r:

$$C = C_0 + rC_1 + \cdots \quad \text{and} \quad \phi = \phi_0 + r\phi_1 + \cdots.$$

In that case the linear theory, to zero order, gives two gravity waves with phase velocity $C_0 = \pm\sqrt{G/K}$ but only the wave with positive C_0 becomes amplified. At the next order, one obtains at the boundary

$$2C_0C_1 = \left[C_0^2\phi_{0,y} + U_{,y}\right] - G, \tag{3.8}$$

and therefore

$$\mathrm{Im}\{C_1\} = \tfrac{1}{2}C\,\mathrm{Im}\{\phi_{0,y}\} \tag{3.9}$$

where ϕ_0 is such that

$$\phi_{0,yy} - \left[K^2 + \frac{U_{,yy}}{U-C_0}\right]\phi_0 = 0. \tag{3.10}$$

A $-\mathrm{i}\pi$ phase change at the critical level is assumed. Due to this phase change, $\phi_{0,y}$ is complex at the interface and thus C_1 has an imaginary component, which is responsible for the instability of the travelling waves.

For the arbitrary r case, the previous expansion does not hold, and one needs to solve the full set of equations (3.1)–(3.4). Alexakis *et al.* (2002) show that the growth

‡ We note that a magnetic field whose direction is aligned with the interface will have the same effect as surface tension, with $\sigma(K) = B^2/(2\pi\mu K)$ (Chandrasekhar 1961).

rate exhibits an exponential dependence on the parameter G. In Appendix A, we carry out an asymptotic analysis for large G, and derive this exponential dependence. More specifically, the growth rate of the most unstable mode is found to be

$$\max(K\ \mathrm{Im}\{C\}) \sim \exp(-2q_m \mathscr{A}_t G), \tag{3.11}$$

where weaker algebraic dependences have been ignored here; $\mathscr{A}_t = (1-r)/(r+1)$ is the Atwood number and $q_m \simeq 2.45\ldots$. The zeroth order of the real part of the phase speed C is $\mathrm{Re}\{C\} = \sqrt{\mathscr{A}_t G/K}$. The exact formula is given in the Appendix (A 31). As is shown there, the stream function Ψ below the critical layer is composed of an exponentially increasing and an exponentially decreasing component. Since the boundary condition (equation (3.2)) must be satisfied, the exponentially large component must be in phase with h, which leaves us with the exponentially small, out-of-phase, component to drive the wave unstable. Further calculation then leads to the result given above.

4. Weakly nonlinear theory

We are now ready to embark upon the weakly nonlinear theory. Formally this is done by assuming that, for some parameter ranges of interests, our physical system lies close to a marginally stable state so that an asymptotic expansion is allowed near the centre manifold. For the problem at hand, however, and in the absence of surface tension ($\mathscr{T} = 0$), marginally stable states are possible only when $r = 0$ or $1/G = 0$; the first one expresses the unphysical situation that there is no upper fluid, and the latter corresponds to a situation where there is no wind in the upper fluid ($U_{max} \sim 1/\sqrt{G}$). Complication arises as we deviate from these neutrally stable states. In ordinary dissipative systems, only a small number of modes near the centre manifold become unstable and need to be considered. In our case though, once the density ratio r or the parameter G is finite, an infinite number of modes become unstable if surface tension $\mathscr{T} = 0$. Ideally the interaction of all these modes needs to be taken into account. Practically, this difficulty is removed by the combined effect of surface tension $\mathscr{T}$ (or, equivalently, the presence of a magnetic field) and weak viscous damping. In the presence of surface tension the stability boundary in the $(r, G, \mathscr{T})$-space is given by the condition for positive solutions of (3.7) and by $r = 0$. Surface tension reduces the number of unstable modes by neutralizing modes of wavenumbers above some cut-off value. Furthermore, weak viscosity will damp out the neutrally stable modes of high wavenumbers, rendering them asymptotically stable. By using a periodic domain, we can fix the period so that only one mode becomes unstable; by doing this we omit wave-packet effects (Maslowe, Benney & Mahoney 1994; Oikawa, Chow & Benney 1987) that would complicate the analysis, and we will therefore ignore them in this first look at the problem. We can then derive the amplitude equation for this single mode as usual.

We focus on situations where $G \gg 1$, corresponding to weak winds or strong gravitation for arbitrary density ratio. As will be shown, the amplitude equations are very similar to those obtained by Reutov (1980) for small density ratios ($r \ll 1$).

In § 3 we showed that unstable modes for the large G case grow at a rate proportional to $\exp\{-2q_m \mathscr{A}_t G t\}$. Inspired by this result, in the limit $G \gg 1$, we set the time derivative $\partial_t = \epsilon \partial_T - C\partial_x$, where the small parameter ϵ (defined later) is such that the linear growth rate (imaginary part of C) is $O(\epsilon)$. We expand the stream function

above the interface as

$$\Psi^+ = \epsilon^2 \Psi_0^+ + \epsilon^3 \Psi_1^+ + \cdots. \tag{4.1}$$

The governing equation (2.2) for the upper fluid is then

$$\epsilon \nabla^2 \Psi^+_{,T} + U \nabla^2 \Psi^+_{,x} - U_{,yy} \Psi^+_{,x} = \Psi^+_{,x} \nabla^2 \Psi^+_{,y} - \Psi^+_{,y} \nabla^2 \Psi^+_{,x} + \nu \nabla^2 \nabla^2 \Psi^+ \tag{4.2}$$

and for the lower fluid

$$\epsilon \nabla^2 \Psi^-_{,T} = \Psi^-_{,x} \nabla^2 \Psi^-_{,y} - \Psi^-_{,y} \nabla^2 \Psi^-_{,x} + \nu \nabla^2 \nabla^2 \Psi^-. \tag{4.3}$$

The boundary conditions at the interface are given by

$$\epsilon h_{,T} - C h_{,x} + \Psi^+_{,x} = \mathrm{NLT}, \qquad \epsilon h_{,T} - C h_{,x} + \Psi^-_{,x} = \mathrm{NLT}, \tag{4.4}$$

$$r[\epsilon \Psi^+_{,Ty} - C \Psi^+_{,xy} - U^+_{,y} \Psi^+_{,x}] - [\epsilon \Psi^-_{,Ty} - C \Psi^-_{,xy}] - [G(1-r)h - \mathscr{T} h_{,xx}] = \mathrm{NLT}, \tag{4.5}$$

where NLT are the nonlinear terms that are of higher order in ϵ. At the zeroth order we have

$$(U - C) \nabla^2 \Psi^+_{0,x} - U_{,yy} \Psi^+_{0,x} = 0;$$

expanding in normal modes, $\Psi_0 = \phi_0(y) \mathrm{e}^{\mathrm{i}Kx} + \text{c.c.}$, we have

$$\phi_{0,yy} - \left[K^2 - \frac{U_{,yy}}{U - C} \right] \phi_0 = 0, \tag{4.6}$$

where we have focused on the most unstable mode. Equation (4.6) is the Rayleigh equation with a singular behaviour at the point y_c where $U(y_c) = C$. The solutions of (4.6) around the critical layer can be expanded in series $\phi_0 \simeq A[1 - (U_c''/U_c')(y - y_c) \times \ln(|y - y_c|) + \cdots] + B[(U_c''/U_c')(y - y_c) + \cdots]$. Of course, the singularity is removed from the real axis if the phase velocity is complex. Nonetheless if the imaginary part of C is of order ϵ (as in the case we now examine), the vorticity perturbation becomes of order $\epsilon^{-1}\epsilon^2 = \epsilon$ near the critical layer, reducing the nonlinear terms to the same order in ϵ as the linear terms, and they have to be taken into account in the asymptotic expansion in the critical layer.

Outside the critical layer the nonlinearity is at higher order ($O(\epsilon^4)$) and can therefore be neglected. It is thus sufficient to use the results from the linear theory for the outer scales. The outer solution (away from the critical layer) can be evaluated numerically. In the case of large G we also have $K \geqslant \mathscr{A}_t G \gg 1$ according to (3.6); thus we can express ϕ_0 using the WKBJ approximation as an asymptotic expansion in terms of $1/K$. An analytic expression for the growth rate can also be obtained in this expansion. We write ϕ_0 as

$$\phi_0 = \begin{cases} A_3 \phi_{above} & \text{if } y > y_c \\ A_1 \phi^+_{below} + B_1 \phi^-_{below} & \text{if } 0 < y < y_c, \end{cases} \tag{4.7}$$

where ϕ_{above} is the exponentially decreasing solution for $y \to +\infty$ and $\phi^{\pm}_{below}$ are the two linearly independent (exponentially increasing and exponentially decreasing) solutions of (4.6). The amplitude coefficients A_1 and B_1 are determined from the inner scaling. In terms of the WKBJ expansion carried out in Appendix A, these solutions

can be written at first order in $1/K$ (note $K \gg 1$), as

$$\phi_0 = \begin{cases} \dfrac{\sqrt{\pi}}{2} A_3 \dfrac{1}{\sqrt{w}} \exp\left(-\displaystyle\int_{y_a}^{y} w\,\mathrm{d}y'\right), & \text{for } y > y_a \\ -\sqrt{\pi} A_3 \cos[I_1] \dfrac{1}{\sqrt{w}} \sin\left(\displaystyle\int_{y_c}^{y} w\,\mathrm{d}y' - \pi/4\right) \\ \quad + \sqrt{\pi} A_3 \sin[I_1] \dfrac{1}{\sqrt{w}} \cos\left(\displaystyle\int_{y_c}^{y} w\,\mathrm{d}y' - \pi/4\right), & \text{for } y_a > y > y_c \\ \sqrt{\pi} A_1 \sin[I_1] \mathrm{e}^{-I_2} \dfrac{1}{\sqrt{w}} \exp\left(+\displaystyle\int_{0}^{y} w\,\mathrm{d}y'\right) \\ \quad + \dfrac{\sqrt{\pi}}{2} B_1 \cos[I_1] \mathrm{e}^{+I_2} \dfrac{1}{\sqrt{w}} \exp\left(-\displaystyle\int_{0}^{y} w\,\mathrm{d}y'\right), & \text{for } y_c > y, \end{cases} \tag{4.8}$$

where I_1 and I_2 are integrals determined from the linear solution and are defined in Appendix A; w is defined in equation (A 6) and y_a is the solution of $w(y) = 0$.

At second order $\Psi_1 = \phi_1 \mathrm{e}^{\mathrm{i}Kx}$ satisfies the inhomogeneous equation

$$\phi_{1,yy} - \left[K^2 - \frac{U_{,yy}}{U - C}\right] \phi_1 = \frac{U_{,yy}}{\mathrm{i}K(U - C)^2} \phi_{0,T} \tag{4.9}$$

which again can be solved numerically. Noting that the inhomogeneous term is of order $1/K^3$ (in the rescaled units $y \to Ky$) everywhere except inside the critical layer, the solutions of (4.9) can be expressed as a WKBJ expansion. For further analysis, it is sufficient to know that below and away from the critical layer, ϕ_1 can be expressed as

$$\phi_1 = A_1^{(1)} \mathrm{e}^{+I_2} \frac{1}{\sqrt{w}} \exp\left(-\int_0^y w\,\mathrm{d}y'\right) + B_1^{(1)} \mathrm{e}^{-I_2} \frac{1}{\sqrt{w}} \exp\left(+\int_0^y w\,\mathrm{d}y'\right).$$

In order to match the outer solution with the solution inside the critical layer we need to know the asymptotic expansion of the outer solution as $y \to y_c$. Following similar calculations as in the linear theory, above the critical layer we have

$$\phi_0 \simeq A_3[\pi \cos[I_1][-z + \cdots] + \sin[I_1][1 - z\ln(z) + \cdots + (1 - 2\gamma)z + \cdots]] \tag{4.10}$$

and

$$\phi_1 \simeq \frac{U_c'' \sin[I_1]\, A_{3,T}}{\mathrm{i}2K U_c'^2} \ln|z| + \cdots \tag{4.11}$$

where $z = (y - y_c)(-U_c'')/U_c'$, γ is the Euler Masceroni constant and the subscript c means evaluated at the critical point. Below the critical layer the asymptotic expansion gives

$$\phi_0 \simeq A_1 \sin[I_1][1 - z\ln|z| + \cdots + (1 - 2\gamma)z + \cdots] + \pi B_1 \cos[I_1] \mathrm{e}^{-I_2}(-z + \cdots) \tag{4.12}$$

and

$$\phi_1 \simeq \frac{U_c'' \sin[I_1]\, A_{1,T}}{\mathrm{i}2K U_c'^2} \ln|z| + \cdots. \tag{4.13}$$

Next we examine the dynamics of the inner scaling in the critical layer.

4.1. *Inner solution*

To capture the dynamics of the critical layer, we use the scaling $\Psi \to \epsilon^2\tilde{\Psi}$, $y - y_c \to \epsilon Y$ and $1/R \to \epsilon^3\nu$. From equation (4.2) we obtain

$$\tilde{\Psi}_{,TYY} + U_c' Y \tilde{\Psi}_{,xYY} + \tilde{\Psi}_{,Y}\tilde{\Psi}_{,YYx} - \tilde{\Psi}_{,x}\tilde{\Psi}_{,YYY} - \nu\tilde{\Psi}_{,YYYY} = -\epsilon\left[\tfrac{1}{2}U_c'' Y^2 \tilde{\Psi}_{,YYx} - U_c''\tilde{\Psi}_{,x}\right] + O(\epsilon^2). \quad (4.14)$$

In order to match with the outer solution (4.10), (4.12) we expand $\tilde{\Psi}$ as

$$\tilde{\Psi} = \tilde{\Psi}_0 + \epsilon\ln(\epsilon)\tilde{\Psi}_1 + \epsilon\tilde{\Psi}_2 + \epsilon^2\ln(\epsilon)\tilde{\Psi}_3 + \epsilon^2\tilde{\Psi}_4 + \ldots. \quad (4.15)$$

To first order, we then have

$$\tilde{\Psi}_{0,TYY} + U_c' Y \tilde{\Psi}_{0,xYY} + \tilde{\Psi}_{0,Y}\tilde{\Psi}_{0,YYx} - \tilde{\Psi}_{0,x}\tilde{\Psi}_{0,YYY} - \nu\tilde{\Psi}_{0,YYYY} = 0.$$

Matching with the outer solution we obtain

$$\tilde{\Psi}_0 = \sin[I_1](A_1 e^{iKx} + A_1^* e^{-iKx}), \quad (4.16)$$

and therefore $A_1 = A_3 \equiv A$. To the next order ($\epsilon\ln(\epsilon)$), we have

$$\tilde{\Psi}_{1,TYY} + U_c' Y \tilde{\Psi}_{1,xYY} - \tilde{\Psi}_{0,x}\tilde{\Psi}_{1,YYY} - \nu\tilde{\Psi}_{1,YYYY} = 0.$$

Matching with the outer solution we obtain

$$\tilde{\Psi}_1 = \left[A\frac{U_c''}{U_c'}Y + \partial_T A\frac{U_c''}{\mathrm{i}2KU_c'^2}\right]\sin[I_1]e^{iKx} + \text{c.c.} \quad (4.17)$$

To third order (ϵ^3), we have

$$\tilde{\Psi}_{2,YYT} + U_c' Y \tilde{\Psi}_{2,YYx} - \tilde{\Psi}_{0,x}\tilde{\Psi}_{2,YYY} - \nu\tilde{\Psi}_{2,YYYY} = U_c''\tilde{\Psi}_{0,x}. \quad (4.18)$$

Denoting $Z = \tilde{\Psi}_{2,YY}$, which is the vorticity inside the critical layer, we obtain

$$Z_{,T} + U_c' Y Z_{,x} - \tilde{\Psi}_{0,x}Z_{,Y} - \nu Z_{,YY} = U_c''\tilde{\Psi}_{0,x}. \quad (4.19)$$

To match with the outer solution, we require the boundary conditions of Z,

$$\lim_{Y\to+\infty} Z = \left[A\frac{U_c''}{U_c'}\frac{1}{Y} - \frac{U_c''}{2\mathrm{i}KU_c'^2}\frac{1}{Y^2}A_{,T}\right]\sin[I_1]e^{iKx} + \text{c.c.},$$

and similarly for $Y \to -\infty$ with A replaced by B_1. Integrating Z along Y and using the asymptotic behaviour of Ψ_2 above and below the critical layer, we obtain

$$\int_{-\infty}^{+\infty} Z\,\mathrm{d}Y = [\Psi_{2,Y}]_{-\infty}^{+\infty} = \pi\frac{U_c''}{U_c'}\cos[I_1][A - B_1]e^{iKx} + \text{c.c.},$$

where we have taken the limiting procedure $\lim_{\epsilon\to0}\int_{-1/\epsilon}^{1/\epsilon} Z\,\mathrm{d}Y$. Defining

$$J \equiv \frac{K}{2\pi\sin[I_1]}\frac{U_c'}{U_c''}\int_{-\pi/K}^{+\pi/K} e^{-iKx}\int_{-\infty}^{+\infty} Z\,\mathrm{d}Y\,\mathrm{d}x. \quad (4.20)$$

we obtain the following important result:

$$\cos[I_1]B_1 = \cos[I_1]A - \frac{1}{\pi}\sin[I_1]J. \quad (4.21)$$

Equation (4.21) implies that the phase change across the critical layer depends on the detailed treatment of the vorticity dynamics inside the critical layer. In the linear

case $J = +\mathrm{i}\pi A$, but as the amplitude grows and the nonlinear term $\tilde{\Psi}_{0,x} Z_{,Y}$ in equation (4.19) becomes important, the phase change will decrease.

4.2. *Boundary conditions and the amplitude equation*

Combining the above results we find that the stream function at the interface is

$$\Psi_0|_0 = \frac{\sqrt{\pi}}{2}\left[A(2\sin(I_1)\mathrm{e}^{-I_2} + \cos(I_1)\mathrm{e}^{+I_2}) - \frac{1}{\pi}J\sin(I_1)\mathrm{e}^{+I_2}\right]\mathrm{e}^{\mathrm{i}K(x-Ct)} + \text{c.c.}, \quad (4.22)$$

$$\Psi_{0,y}|_0 = \frac{\sqrt{\pi}}{2}K\left[A\left(2\sin(I_1)\mathrm{e}^{-I_2} - \cos(I_1)\mathrm{e}^{+I_2}\right) + \frac{1}{\pi}J\sin(I_1)\mathrm{e}^{+I_2}\right]\mathrm{e}^{iK(x-Ct)} + \text{c.c.}, \quad (4.23)$$

Unlike the linear case, the phase change is now defined by J in equation (4.20). The slow time scale mentioned before is defined by the value of C_i, which is exponentially small and is given by equation (3.11). We therefore define $\epsilon \equiv \mathrm{e}^{-2I_2} \sim \mathrm{e}^{-2G}$, and equations (4.22) and (4.23) can be re-written as

$$\Psi_0|_0 = \frac{\sqrt{\pi}}{2}\left[\frac{1}{\sqrt{\epsilon}}A\cos(I_1) - \frac{1}{\sqrt{\epsilon}\pi}J\sin(I_1) + 2\sqrt{\epsilon}A\sin(I_1)\right]\mathrm{e}^{\mathrm{i}Kx} + \text{c.c.} \quad (4.24)$$

To match with the upper fluid we expand Ψ^- and h as

$$\Psi^- = \epsilon^{3/2}\Psi_0^- + \epsilon^{5/2}\Psi_1^- + \cdots \quad \text{and} \quad h = \epsilon^{3/2}h_0 + \epsilon^{5/2}h_1 + \cdots.$$

We write the zeroth-order stream function Ψ_0^- below the interface, and the surface elevation h_0 as $\Psi_0^- = CH\mathrm{e}^{\mathrm{i}Kx+Ky} + \text{c.c.}$ and $h_0 = H\mathrm{e}^{\mathrm{i}Kx} + \text{c.c.}$, H being the amplitude of the wave.

The first-order ($\epsilon^{3/2}$) boundary conditions give us $\boldsymbol{M}\cdot\boldsymbol{V}_0 = 0$, where

$$\boldsymbol{M} = \begin{bmatrix} -C & 1 & 0 \\ -C & 0 & 1 \\ -\tilde{G}(1-r) & rCK & CK \end{bmatrix} \quad \text{and} \quad \boldsymbol{V}_0 = \begin{bmatrix} H \\ \Phi \\ CH \end{bmatrix}. \quad (4.25)$$

$\Phi = (A\cos(I_1) - (1/\pi)J\sin(I_1))$ is the amplitude of the stream function at the interface and $\tilde{G} = G + K^2\mathscr{T}/(1-r)$ is the gravity term including the effect of surface tension. Here we discard the $U_{,y}$ term since it is of order $1/K$. For a non-trivial solution, we must have $\det(M) = 0$. This leads us to the relation $C = \sqrt{\tilde{G}\mathscr{A}_t/K}$ and $HC = \Phi$.

At the next order, we have ϕ_1 at the interface:

$$\phi_1|_0 = A_1^{(1)}\frac{1}{\sqrt{\epsilon}} + B_1^{(1)}\sqrt{\epsilon} \quad \text{and} \quad \phi_{1,y}|_0 = -KA_1^{(1)}\frac{1}{\sqrt{\epsilon}} + KB_1^{(1)}\sqrt{\epsilon} \quad (4.26)$$

where the values of $A_1^{(1)}, B_1^{(1)}$ depend on $A_{,T}$, and can be obtained by matching with the inner solution at the critical layer. The second term in equation (4.26) is exponentially small (of order $\sqrt{\epsilon}$) and can thus be neglected. The stream function of the lower fluid Ψ_1^- and the elevation h_1 at this order are $\Psi_1^- = CH^{(1)}\mathrm{e}^{\mathrm{i}Kx+Ky} + \text{c.c.}$ and $h_1 = H^{(1)}\mathrm{e}^{\mathrm{i}Kx} + \text{c.c.}$ The boundary conditions at the interface are

$$\boldsymbol{M}\cdot\boldsymbol{V}_1 = -\frac{1}{\mathrm{i}K}\partial_T\boldsymbol{W}_1 + \boldsymbol{W}_2 \quad (4.27)$$

(where $\boldsymbol{M}$ was defined in equation (4.25)),

$$\boldsymbol{V}_1 = \begin{bmatrix} H^{(1)} \\ \Phi_1 A_1^{(1)} \\ CH^{(1)} \end{bmatrix}, \quad \boldsymbol{W}_1 = \begin{bmatrix} H \\ H \\ -K(r\Phi + CH) \end{bmatrix} = H\begin{bmatrix} 1 \\ 1 \\ -(r+1)KC \end{bmatrix}, \quad (4.28)$$

and

$$\boldsymbol{W}_2 = \begin{bmatrix} -2\sin(I_1)A \\ 0 \\ 2rKC\sin(I_1)A \end{bmatrix}. \tag{4.29}$$

We define $\boldsymbol{V}^T \equiv [-rCK, -CK, 1]$ where $\boldsymbol{V}^T$ is such that $\boldsymbol{V}^T \cdot \boldsymbol{M} = 0$. Multiplying equation (4.27) with $\boldsymbol{V}^T$, we obtain $\boldsymbol{V}^T \boldsymbol{W}_1 = -2(1+r)CKH$ and $\boldsymbol{V}^T \cdot \boldsymbol{W}_2 = 4rCKH\sin(I_1)$. Hence, we arrive at the amplitude equation for large G:

$$\frac{1}{\mathrm{i}K}\boldsymbol{V}^T \cdot \boldsymbol{W}_{1,T} = \boldsymbol{V}^T \cdot \boldsymbol{W}_2 \quad \text{or} \quad H_{,T} = -\mathrm{i}K\frac{2r}{1+r}\sin(I_1)A, \tag{4.30}$$

with

$$CH = 2A\cos(I_1) - J\frac{1}{\pi}\sin(I_1). \tag{4.31}$$

The amplitude evolution can now be determined from equations (4.30)–(4.31).

Equations (4.30)–(4.31) can be re-written in more familiar form

$$H_{,T} = -\mathrm{i}\mathscr{C}_1 H + \mathscr{C}_2 J, \tag{4.32}$$

$$H = \mathscr{D}_1 A + \mathscr{D}_2 J, \tag{4.33}$$

where $\mathscr{C}_1, \mathscr{C}_2, \mathscr{D}_1, \mathscr{D}_2$ are coefficients determined from the solutions of the linear problem. Equations (4.32)–(4.33), along with the definition of J in equation (4.20), were first found (in an equivalent form) by Reutov (1980) to describe the weakly nonlinear evolution of a single wave coupled to the vorticity in an inviscid critical layer, for small density ratio $r \equiv \epsilon \ll 1$, with G of order one. If the viscosity is included in his treatment by scaling viscosity $\nu \to \epsilon^3\nu$, the same equation for vorticity Z can be obtained, and his amplitude equations for $r \ll 1$ and unity G take exactly the same form as our amplitude equations for the $G \gg 1$ case. We thus focus on the general form of the amplitude equations in the next section, and present results from solving equations (4.19), (4.20) and (4.32)–(4.33). We note here that Reutov pointed out the fact that with the extra assumption $\mathscr{D}_2 = 0$ equations (4.32)–(4.33) are identical with those describing electrostatic waves in a plasma, which have already been solved numerically by Onishchenko *et al.* (1970). We investigate the properties of the full set of equations without this assumption in the next section.

5. Results

5.1. *Preliminaries*

For both cases (weak wind and small density ratio), the amplitude equations can be cast into the following more general form:

$$H_{,T} + \mathrm{i}\mathscr{C}_1 H = \mathrm{i}\mathscr{C}_2 J, \tag{5.1}$$

$$H = \mathscr{D}_1 A + \mathscr{D}_2 J, \tag{5.2}$$

$$J = \frac{K}{2\pi}\frac{U_c'}{U_c''}\int_{-\pi/K}^{+\pi/K} \mathrm{e}^{-\mathrm{i}Kx}\int_{-\infty}^{+\infty} Z\,\mathrm{d}Y\,\mathrm{d}x \equiv \langle \mathrm{e}^{-\mathrm{i}Kx} Z\rangle, \tag{5.3}$$

$$Z_{,T} + U_c' Y Z_{,x} - \tilde{\Psi}_{0,x} Z_{,Y} - \nu Z_{,YY} = U_c''\tilde{\Psi}_{0,x}, \tag{5.4}$$

with

$$\lim_{Y\to\infty} Z = \left[A\frac{U_c''}{2U_c'}\frac{1}{Y} + \frac{U_c''}{2U_c'^2}\frac{1}{Y^2}A_{,T}\right]\mathrm{e}^{\mathrm{i}Kx} + \text{c.c.} \tag{5.5}$$

and

$$\tilde{\Psi}_0 = (A\mathrm{e}^{\mathrm{i}Kx} + A^*\mathrm{e}^{-\mathrm{i}Kx}), \tag{5.6}$$

where the coefficient $\sin[I_1]$ from (4.16) has been absorbed in the amplitude A in (5.6).

The above equations can be interpreted as follows. Equation (5.2) expresses the continuity of the normal velocity at the interface: it imposes the constraint that the phase and amplitude of the perturbation of the surface wave (given by H) is the same as the perturbation of the wind (given by $\mathscr{D}_1 A + \mathscr{D}_2 J$) including the component that comes from the phase change at the interface. Equation (5.1) is Newton's law, or alternatively can be viewed as a statement about the continuity of pressure at the interface; it gives the growth of the amplitude H due to the out-of-phase component of the pressure. Equation (5.4) gives the evolution of the vorticity inside the critical layer that determines the phase change, and involves the nonlinear term $\tilde{\Psi}_{0,x} Z_{,Y}$. The coefficients $\mathscr{C}_1, \mathscr{C}_2, \mathscr{D}_1, \mathscr{D}_2, \in \Re$ are obtained from the linear theory, and are given in equations (4.16), (4.30) and (4.31). $\mathscr{C}_1$ and $\mathscr{D}_2$ are coefficients that involve correction to the real part of C due to both the gradient of the velocity at the interface $U_{,y}$ and the pressure component in phase with the travelling wave. $\mathscr{C}_2$ and $\mathscr{D}_1$ involve the part of the pressure perturbation that is out of phase with the travelling wave.

Before we start investigating the properties of the set of equations (5.1)–(5.4) we re-scale the amplitudes, the time scale and length scales to reduce the number of free parameters. The rescaling is carried out in Appendix B, where it is shown that we can set $\mathscr{C}_1 = 0$ and $\mathscr{D}_1 = -\mathscr{C}_2 = U' = U'' = K = 1$ with no loss of generality. The two remaining independent parameters are $\mathscr{D}_2$ and ν.

Dropping the nonlinear term in (5.4) we obtain $J = \mathrm{i}\pi A$ in the linear case (Drazin & Reid 1981). Assuming an exponential growth rate $A = \mathrm{e}^{\gamma T} a_1$ and $H = \mathrm{e}^{\gamma T} a_2$, equation (5.4) can be written as

$$\left.\begin{aligned} \gamma a_2 - \pi a_1 &= 0, \\ a_2 - (1 + \mathrm{i}\pi\mathscr{D}_2) a_1 &= 0; \end{aligned}\right\} \tag{5.7}$$

the growth rate then is given by

$$\gamma = \frac{\pi}{1 + \pi^2 \mathscr{D}_2^2} - \mathrm{i}\frac{\pi^2 \mathscr{D}_2}{1 + \pi^2 \mathscr{D}_2^2}. \tag{5.8}$$

We note as an aside that there are several conservation laws at work here. First, the vorticity is conserved inside the critical layer $\langle Z \rangle_{,T} = 0$, which implies $\langle Z \rangle = 0$ since the initial Z had infinitesimal amplitude. Second, by noting that $\langle \Psi_{0,x} Z \rangle = \mathrm{i}K(J^* A - J A^*)$, one can show that the following laws hold:

$$\frac{\mathrm{d}}{\mathrm{d}T}\{|H|^2 + \langle YZ \rangle\} = 0, \tag{5.9}$$

$$\frac{\mathrm{d}}{\mathrm{d}T}\left\{|H|^2 - \tfrac{1}{2}\langle Z^2 \rangle\right\} = \nu \langle Z_{,Y}^2 \rangle, \tag{5.10}$$

$$\frac{\mathrm{d}}{\mathrm{d}T}\left\{\left\langle \left(\tilde{\Psi}_0 + \tfrac{1}{2}Y^2\right) Z \right\rangle + \mathscr{D}_2 |J|^2\right\} = \nu \langle Z \rangle. \tag{5.11}$$

Equations (5.10) and (5.11) are conservation laws only if $\nu = 0$. In equations (5.9), (5.10) and (5.11), the integration over x was assumed to be taken first, so that we ensure the convergence of the integrals. Recalling that the velocity (in the units we are using) inside the critical layer is given by $[u - C, w] = [\epsilon Y + \epsilon^2(1/2Y^2 +$

$\Psi_{2,Y}) + \cdots, \epsilon^2\Psi_{0,x} + \cdots]$ we can identify the first relation (5.9) as corresponding to the conservation of momentum. Combining equations (5.9) and (5.10), we obtain the conservation of enstrophy inside the critical layer,

$$\frac{\mathrm{d}}{\mathrm{d}T}\langle Z^2\rangle = -\nu\langle Z_{,Y}^2\rangle. \tag{5.12}$$

The third equation (5.11) can be regarded as a statement of the conservation of energy.

5.2. *Quasi-steady state*

An interesting limit in our set of equations is when the rescaled viscosity is large enough to play a dominant role inside the critical layer. With this assumption we can drop the time derivative term in equation (5.4)†; Z then depends only on the value of A, which then makes J a function of A only. More specifically we have

$$\nu Z_{,YY} + \tilde{\Psi}_{0,x} Z_{,Y} - Y Z_{,x} = -\tilde{\Psi}_{0,x}; \tag{5.13}$$

by letting $A = R(T)\mathrm{e}^{\mathrm{i}\Theta(T)}$, $\xi = x + \Theta$ and also using the rescaling $Y = \sqrt{2}\eta R^{1/2}$, $Z = \sqrt{R/2}\hat{Z}(\xi, \eta)$ and $\chi \equiv \nu/(2R)^{3/2}$, we obtain

$$\chi \hat{Z}_{,\eta\eta} - \sin(\xi)\hat{Z}_{,\eta} - \eta \hat{Z}_{,\xi} = 2\sin(\xi). \tag{5.14}$$

Equation (5.3) then becomes

$$J = \frac{1}{2\pi} R\mathrm{e}^{\mathrm{i}\Theta} \int_{-\infty}^{+\infty} \int_{-\pi+\Theta}^{+\pi+\Theta} \mathrm{e}^{-\mathrm{i}\xi} \hat{Z}\, \mathrm{d}\xi\, \mathrm{d}\eta = -\mathrm{i}\frac{1}{2\pi} A \int_{-\infty}^{+\infty} \int_{-\pi}^{+\pi} \sin\xi\, \hat{Z}\, \mathrm{d}\xi\, \mathrm{d}\eta, \tag{5.15}$$

where the $\cos(\xi)$ term is zero due to symmetry. Equation (5.15) can be written as

$$J = -\mathrm{i}A\Phi_H(\chi), \text{ with } \Phi_H(\chi) = \frac{1}{2\pi} \int_{-\pi}^{+\pi} \int_{-\infty}^{+\infty} \sin\xi\, \hat{Z}\, \mathrm{d}\eta\, \mathrm{d}\xi. \tag{5.16}$$

$\Phi_H(\chi)$ was first studied numerically by Haberman (1972). Its value ranges from $-\pi$ for $\chi \to \infty$ to 0 for $\chi \to 0$. Its asymptotics for $\chi \to 0$ and $\chi \to \infty$ are given by

$$\Phi_H(\chi) = \begin{cases} -c_1\chi + c_2\chi^{3/2} + O(\chi^2), & \chi \ll 1, \\ -\pi + c_3\chi^{-4/3} + O\left(\chi^{-8/3}\right), & \chi \gg 1, \end{cases} \tag{5.17}$$

where $c_1 = 5.5151\ldots$, $c_2 = 4.2876\ldots$ and $c_3 = 1.6057\ldots$. The derivation for the above asymptotics can be found in Churilov & Shukhman (1996). The amplitude equation then can be written as

$$H_{,T} = -A\Phi_H\left(\frac{\nu}{(2|A|)^{3/2}}\right), \text{ with } H = A + \mathrm{i}\mathscr{D}_2 A\Phi_H\left(\frac{\nu}{(2|A|)^{3/2}}\right).$$

We have thus ended up with an ordinary differential equation for the amplitude of the wave. Writing A in terms of R and Θ, and after some algebra, one can show that

$$\left(1 + \mathscr{D}_2^2\Phi_H\tilde{\Phi}_H\right)R_{,T} = -R^2\Phi_H, \text{ and } \left(1 + \mathscr{D}_2^2\Phi_H\tilde{\Phi}_H\right)\Theta_{,T} = -\mathscr{D}_2\Phi_H\tilde{\Phi}_H, \tag{5.18}$$

where $\tilde{\Phi}_H = (R\Phi_H)_{,R}$. For large R at late times we can conclude that

$$|H| \sim |A| \equiv R \sim \nu T^{2/3} \quad \text{and} \quad \Theta \sim \nu^2 T^{-1}. \tag{5.19}$$

† By using the rescaling $A \to \nu^{2/3}A$, $Z \to \nu^{1/3}Z$, $Y \to \nu^{1/3}Y$ one can show that the time derivative term is of order $\nu^{-1/3}$ smaller than the other terms.

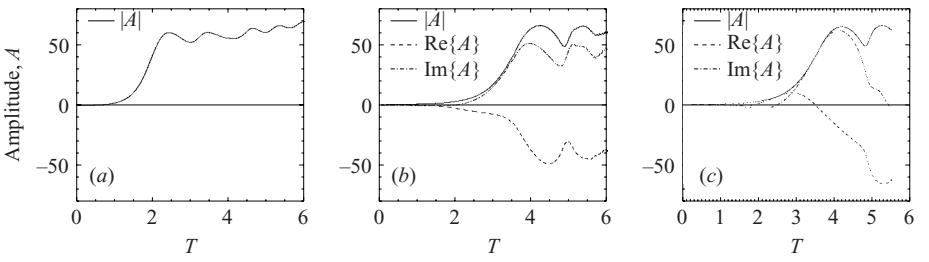

FIGURE 1. The evolution of the wave amplitude A for (a) $\mathscr{D}_2 = 0$, (b) $\mathscr{D}_2 = +0.3$, (c) $\mathscr{D}_2 = -0.3$.

This is one of the basic results of our calculations. The above limit becomes valid at later times when small scales appear inside the critical layer, even when the rescaled viscosity is smaller than one. An important implication of this result is that the amplitude grows with an algebraic power instead of the initial exponential variation. Another important feature is that the growth rate depends linearly on the viscosity, unlike the case in linear theory. In linear theory, a weak viscosity gave the same phase change '$-\mathrm{i}\pi$', and the resulting growth rate was independent (to first order) of ν. Finally we note that the phase of the waves, Θ, goes asymptotically to zero at late times.

5.3. *Numerical results*

Next we investigate the weakly nonlinear evolution of the wave by solving equations (5.1)–(5.4) numerically. To solve the advection equation (5.4), we used a code which is spectral in x and finite difference in Y. The domain range we used was $(-50, 50)$ in Y and $(0, 2\pi)$ in x. Up to 1024 grid points were used in the Y-direction and 63 modes were kept in x. Viscosity $\nu = 0.1$ is used in all the simulations. The far-field boundary conditions ($Y \to \pm\infty$) were satisfied to order $1/Y$, although the asymptotic behaviour of Z was taken into account when we evaluated the integral in equation (5.3). The code was tested by comparing with a fully pseudo-spectral code as well as with already published results.

Equations involving a critical layer have been solved numerically for various cases (Balmforth & Young 2002; Balmforth & Piccolo 2001; Goldstein & Hultgren 1988; Warn & Warn 1978; Onishchenko *et al.* 1970). The nonlinear evolution of the critical layer leads to the well-studied 'cats-eye' pattern. As the amplitude of the wave increases, the 'phase-change' across the critical layer is decreased to zero and the amplitude saturates up to diffusive time scales. We will focus only on the differences introduced by the coupling of the amplitude A of the upper 'wind' perturbation with the amplitude of the wave H. Such coupling is controlled by the parameter $\mathscr{D}_2$. When $\mathscr{D}_2 = 0$ we have no feedback of the gravity wave to the critical layer 'free critical layer'; the amplitude A then is proportional to H. In figure 1 we plot the amplitude of the 'wind perturbation' A as a function of time for three different cases: $\mathscr{D}_2 = 0, \pm 0.3$. The saturation amplitude does not seem to strongly depend on the coupling coefficient $\mathscr{D}_2$. The phase of the amplitude ($\arg\{A\}$) does change; this corresponds to travelling vortices.

Figure 2(a) shows the temporal behaviour of the phase change $\mathrm{Im}\{-J/A\}$, which is similar for all three cases. Panels (b) and (c) show the evolution of the amplitude of the wave H as a function of time for the $\mathscr{D}_2 = \pm 0.3$ cases. H has the same properties as A although the time dependence is smoother, which is expected since H can be written as a time integral of A.

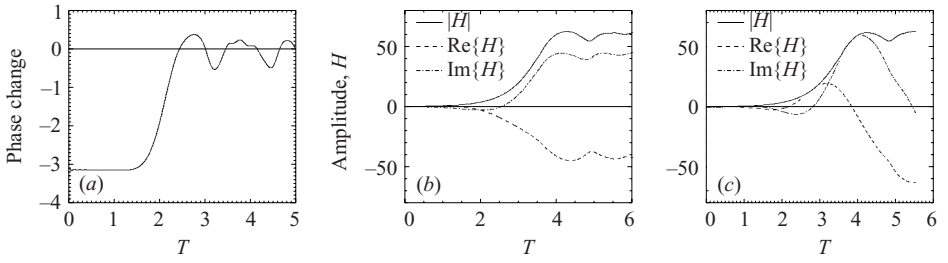

FIGURE 2. The evolution of the phase change across the critical layer as a function of time for the $\mathscr{D}_2 = 0$ case (a), and the evolution of the wave amplitude H for the cases $\mathscr{D}_2 = +0.3$ (b) and $\mathscr{D}_2 = -0.3$ (c).

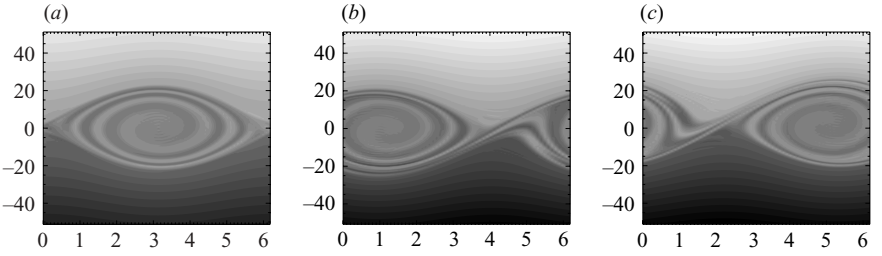

FIGURE 3. Plots of the vorticity inside the critical layer using a grey-scale representation for the cases $\mathscr{D}_2 = 0, +0.3, -0.3$ (a–c respectively) at $T = 4.5$, 5.0 and 5.

Finally in figure 3 we display the total vorticity $Z + Y$ inside the critical layer at the nonlinear stage, for the cases $\mathscr{D}_2 = 0, \pm 0.3$. The displacement of the vortices in the non-zero coupling coefficient cases indicates that the vortices are drifting with respect to the frame co-moving with the wave. Furthermore, we note the small differences in the vorticity near the separatrix between figure 3(a) and figures 3(b) and 3(c). This hints at different mixing properties induced by the coupling with the wind, which turn out to be important in the mixing properties of the flow that we examine in the next section.

6. Effect of gravity wave on chaotic mixing inside critical layers

The above analysis was originally motivated by the possibility of enhanced mixing of different fluids due to the instability of wind-driven gravity waves at the interface. Specifically in the context of nuclear runaway in novae, we are ultimately most interested in the mixing of two differentially rotating layers of distinct chemical abundances in a strong gravitational field (Rosner *et al.* 2001). In the strongly nonlinear regime, where the surface waves break due to the wind, dimensional analysis based on preliminary numerical simulations (Rosner *et al.* 2001 and references therein) indicates that turbulent mixing due to breaking of wind-driven gravity waves is the key to explaining the mixing of white dwarf stellar matter into the 'burning' accreted envelope on time scales consistent with the observations. Motivated by these results, we investigate in this section the effect of gravity waves on the chaotic mixing in the critical layers, before wave breaking occurs. In this case, the weakly nonlinear flow is laminar everywhere, as shown in previous section; and the cat's eye vortices develop within the critical layer, with the gravity surface waves yet too weak to break. Fortunately, there already exists a substantial body of work focused on mixing within

critical layers. The aim of this section is to analyse weakly nonlinear wave-driven mixing from this perspective; we mainly focus on the qualitative aspects, and illustrate how the coupling between gravity waves and vorticity inside the critical layer alters the mixing.

Similar chaotic mixing in critical layers associated with Rossby waves has been investigated in great detail, using a variety of approaches, and in various geophysical and plasma physics contexts (del Castillo-Negrete & Morrison 1993; Ngan & Shepherd 1997; del Castillo-Negrete 2000). Proper treatment of the mixing in the critical layer requires consistency in updating the velocity field, vorticity and the tracer particles (del Castillo-Negrete 2000). The sensitivity of transport of tracer particles to their initial conditions reflects the complicated structures of manifolds commonly found in these non-integrable Hamiltonian systems (del Castillo-Negrete & Morrison 1993; Ngan & Shepherd 1997).

In the previous section, we have found that, with or without coupling with surface waves, the general flow structure of the vortices is similar inside the critical layer. Such vortical structures are typical of the weakly nonlinear evolutions of parallel flows (del Castillo-Negrete 2000; Balmforth & Piccolo 2001). However, their mixing properties may be very different (depending on the details of the underlying flow) in spite of great similarity in the general features. As pointed out in del Castillo-Negrete & Morrison (1993), the single-wave approach adopted above to derive the amplitude equations is equivalent to the pendulum approximation of a single-mode Hamiltonian system. In our amplitude equation (5.4), the vorticity Z is advected by a time-dependent pendulum flow: $(u, v) = (Y, -\Psi_{0,x})$, with $\Psi_0 \equiv A\mathrm{e}^{\mathrm{i}Kx} + \text{c.c.}$ Putting $A \equiv R(T)\mathrm{e}^{\mathrm{i}\Theta(T)}$, the particle trajectories $(x(\boldsymbol{x}_0; T), Y(\boldsymbol{x}_0; T))$ satisfy equations

$$x_{,T} = u = Y, \tag{6.1}$$

$$Y_{,T} = v = K R(T) \sin(Kx + \Theta(T)), \tag{6.2}$$

where $\boldsymbol{x}_0 \equiv (x_0, Y_0)$ is the initial particle position.

Given the time dependence from the numerical solutions in the previous section, we can calculate the strain rate of such a flow by first linearizing equations (6.1)–(6.2) for an infinitesimal separation between two particles $\delta\boldsymbol{x}$,

$$\frac{\mathrm{d}\delta\boldsymbol{x}}{\mathrm{d}T} = (\delta\boldsymbol{x}\cdot\nabla)\mathbf{v} = \begin{pmatrix} 0 & 1 \\ K^2 R\cos(Kx(\boldsymbol{x}_0; T) + \Theta) & 0 \end{pmatrix} \delta\boldsymbol{x} \equiv \boldsymbol{A}\delta\boldsymbol{x}. \tag{6.3}$$

λ_0, defined as the product of eigenvalues of matrix $\boldsymbol{A}$ in equation (6.3), is interpreted as the combination of strain and rotation: $\lambda_0(\boldsymbol{x}_0) = -\det(\boldsymbol{A}) = R\cos(Kx(\boldsymbol{x}_0; T) + \Theta)$. During the numerical integration of equations (5.1)–(5.4) from $t = 0$ to $t \sim 8$, we update λ_0 for each $\boldsymbol{x}_0$ in the computation domain as the amplitudes are updated, and we obtain λ_0 as a function of both space $(\boldsymbol{x}_0)$ and time. We then time-average λ_0 for each $\boldsymbol{x}_0$ in the entire domain. The time-averaged λ_0, denoted as $\langle\lambda_0\rangle$, is a function of only the initial position $\boldsymbol{x}_0$ of the particle. Positive $\langle\lambda_0\rangle$ implies the likelihood of a positive Lyapunov exponent for that initial position; negative $\langle\lambda_0\rangle$ implies that rotation is dominant over strain. We have calculated the time-averaged $\langle\lambda_0\rangle$ for each initial position $\boldsymbol{x}_0$ in the computation domain for $\mathscr{D}_2 = 0.2$ case as shown in figure 4(*b*). Figure 4(*b*) is to be compared with figure 4(*a*), where the vorticity is decoupled from the surface wave: $\mathscr{D}_2 = 0$. More striated layers are found in figure 4(*b*), indicating more complicated tangles of manifolds due to coupling with the surface gravity wave.

The relation between $\langle\lambda_0\rangle$ and the finite-time Lyapunov exponent may not be straightforward, and can depend sensitively on the prescribed flow. In general cases

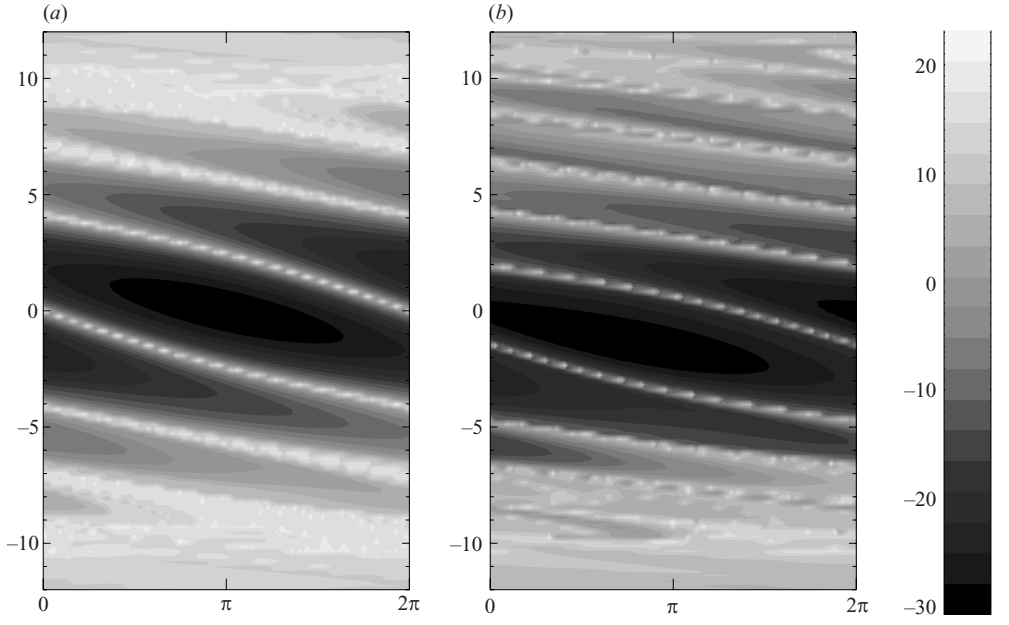

FIGURE 4. (*a*) $\langle\lambda_0\rangle$ for the critical layer without coupling to the gravity wave ($\mathscr{D}_2 = 0$). (*b*) $\langle\lambda_0\rangle$ for the critical layer coupled to the gravity wave ($\mathscr{D}_2 = 0.2$). Bright regions indicate possible positive Lyapunov exponent.

where the flow is time dependent, some correction to $\langle\lambda_0\rangle$ can be made so that it is closer to the Lagrangian description (Boffetta *et al.* 2001):

$$\langle\lambda\rangle = \langle\lambda_0\rangle + \langle\lambda_1\rangle, \tag{6.4}$$

$$\lambda_1 = \sqrt{\Psi_{,Txy}^2 - \Psi_{,Txx}\Psi_{,Tyy}}, \tag{6.5}$$

where Ψ is the stream function of the flow. Interestingly $\lambda_1 = 0$ in our case despite the time-dependence of the amplitudes. Thus we expect $\langle\lambda_0\rangle$ to be a good indicator of the finite-time Lyapunov exponent, which we have also calculated independently (figure 5) for the two corresponding cases in figures 4(*a*) and 4(*b*). Similar to dynamical systems, positive finite-time Lyapunov exponents strongly suggest the presence of unstable mixing manifolds. The larger the number of positive finite-time Lyapunov exponents in the system, the more chaotic is the mixing.

The spatial distribution of the finite-time Lyapunov exponents (FTLE) is certainly different between figures 5(*a*) and 5(*b*) due to the coupling of shear flow to the surface wave. However, up to time $T \sim 8$, our calculation shows that the range of positive FTLE is similar: both cases have almost identical maximum ($\sim$0.72) and minimum (~ -0.4) values. The relative frequency of positive FTLE is also similar (see figure 6), with a slight difference in the variance: variance $\sim$0.04 in (*b*), while in (*a*) variance $\sim$0.03.

In realistic situations where the passive tracers may be weakly diffusive, the asymptotic mixing property is determined by the combination of slow diffusion and fast advection. If we define ζ as the tracer concentration, we can write down the equation for the weakly diffusive tracer in the above flow field (6.1) and (6.2) as

$$\zeta_{,T} + Y\zeta_{,x} + R(T)\sin(Kx + \Theta(T))\zeta_{,Y} = \frac{1}{Pe}\nabla^2\zeta, \tag{6.6}$$

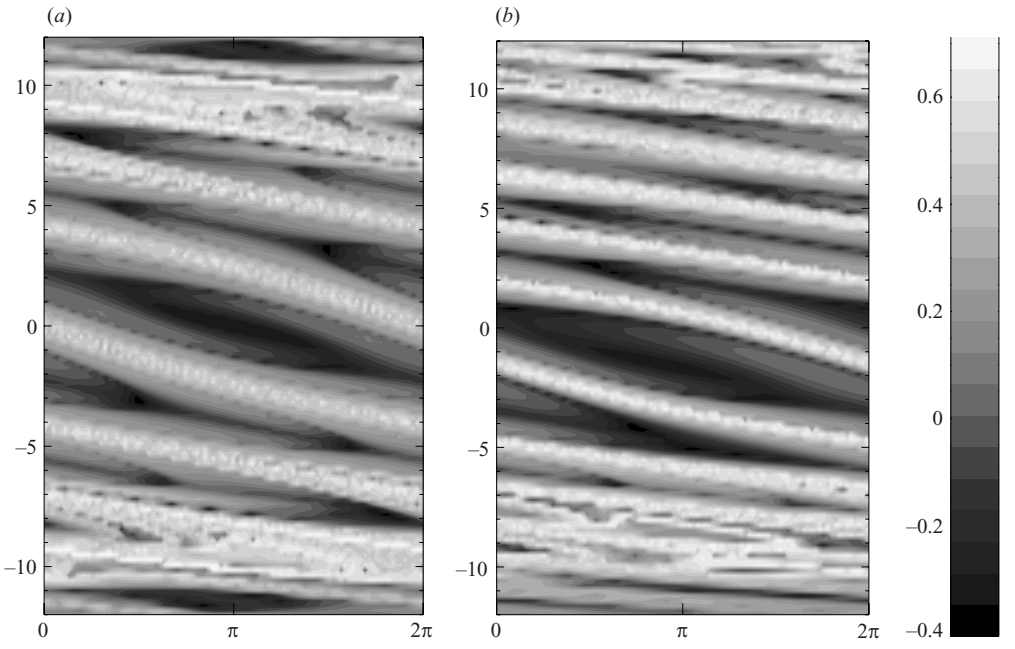

FIGURE 5. (*a*) Finite-time Lyapunov exponent the uncoupled case $\mathscr{D}_2 = 0$. (*b*) Finite-time Lyapunov exponent for the case $\mathscr{D}_2 = 0.2$. Bright regions indicate positive Lyapunov exponent.

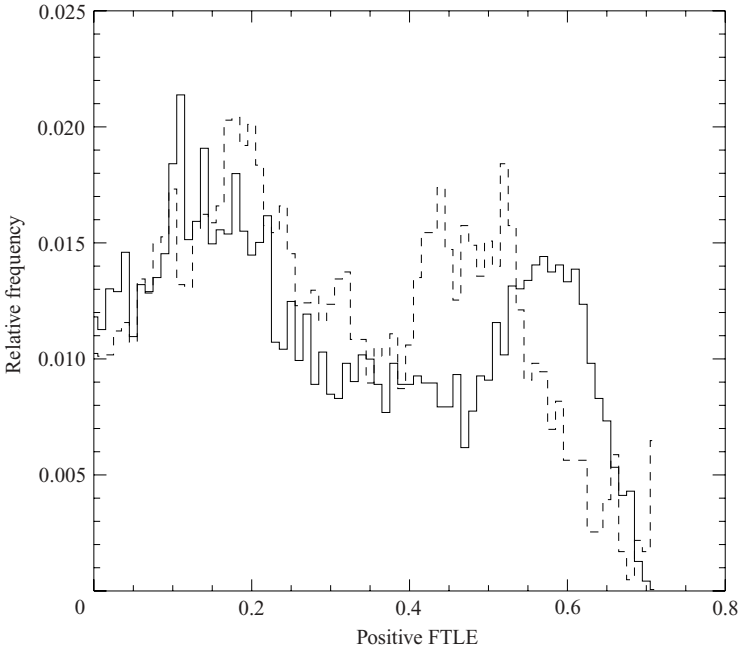

FIGURE 6. Probability distribution of the positive finite-time Lyapunov exponent. Dashed line corresponds to figure 5(*a*), and solid line corresponds to figure 5(*b*).

where $Pe \equiv U_{max} l/\kappa$ is the Péclet number, with U_{max} and l the characteristic velocity and length defined in the previous section, and κ the molecular diffusivity of the tracer. Among all the measures used to describe mixing of diffusive tracers in shear

flows, we focus on the streamwise particle dispersion (variance), defined as

$$\sigma^2 \equiv \langle x^2 \rangle - \langle x \rangle^2, \tag{6.7}$$

where $\langle x \rangle$ and $\langle x^2 \rangle$ are, respectively, the first and second longitudinal moments of the concentration field ζ:

$$\langle x \rangle \equiv \int x\zeta \, \mathrm{d}^2x, \;\; \langle x^2 \rangle \equiv \int x^2\zeta \, \mathrm{d}^2x,$$

and we similarly define the y-variance $\sigma_y^2 \equiv \langle y^2 \rangle - \langle y \rangle^2$.

If the flow is weak and diffusion is strongly dominant over advection, particles undergo random walks and σ increases linearly with the square root of time: $\sigma = (2T/Pe)^{1/2}$. On the other hand, if the shear flow is strong and irregular in time, the particles will be in a super-diffusive regime ($\sigma \sim T^\alpha$, $\alpha > 1$), during which the dispersion grows faster than that for ballistic transport ($\sigma \sim T$). In cases where the flow is bounded and time-independent, the super-diffusive regime eventually gives way to yet another diffusive (Taylor) regime, with a larger effective diffusivity than molecular diffusion (Latini & Bernoff 2001). For a time-dependent velocity field, the super-diffusive regime is the long-time limit of particle transport.

To examine how the time dependence of the flow affects diffusive particle mixing in our case, we have integrated equation (6.6) using a particle method (Latini & Bernoff 2001 and references therein). Due to the need to integrate equation (6.6) over long durations, we have used three models of $R(T)$ and $\Theta(T)$, resembling two classes of solutions from solving the amplitude equations (figure 7); the first two are for the inviscid critical layer, where the amplitude oscillates around the saturated value, while the third is for a viscous critical layer, where the amplitude grows as $T^{2/3}$ asymptotically in time.

We place 10^5 particles at an initial position close to the separatrix, solve for their positions in $\Re^2$, according to equation (6.6) for $Pe = 10^5$, and record their positions, from which we can calculate the particle dispersion. As pointed out in Latini & Bernoff (2001), the method used (Lingevitch & Bernoff 2001) is particularly robust for small values of the diffusion coefficient, e.g. large Péclet number. In our case (equations (6.1) and (6.2)), ballistic transport is expected (and confirmed numerically) if there is no time variation in A.

Figure 7 illustrates the temporal characteristics of the model flow amplitudes R we used in this study: two cases corresponding to inviscid critical layers, for which the initially exponentially growing amplitude saturates to $R \sim 1$ at $T \sim 100$ and then oscillates periodically with a fluctuation amplitude of 0.2 and periods of 6 and 65, respectively; and one case corresponding to the viscous situation, in which the amplitude oscillation just discussed is replaced by an algebraic growth proportional to $T^{2/3}$. The consequent results for our measured transverse and longitudinal particle dispersion are shown in figure 8, which provides the computed dispersion σ versus time for these three cases. We clearly see that the early time dependence of σ is verified as the diffusive regime, where $\sigma = (2T/Pe)^{1/2}$; and that transverse diffusion saturates, corresponding to complete transverse mixing in the critical layer. We also observe that the long-time asymptotics for all cases studied are at least super-diffusive, with $\sigma \sim T^{3/2}$ for cases 1 and 2, while for case 3, where the amplitude grows as $T^{2/3}$, the dispersion is close to $\sigma \sim T^2$. This contrasts with results for Poiseuille flow, for which longitudinal diffusion asymptotes to Taylor dispersion once transverse diffusion saturates (Latini & Bernoff 2001); this difference in behaviour is expected because

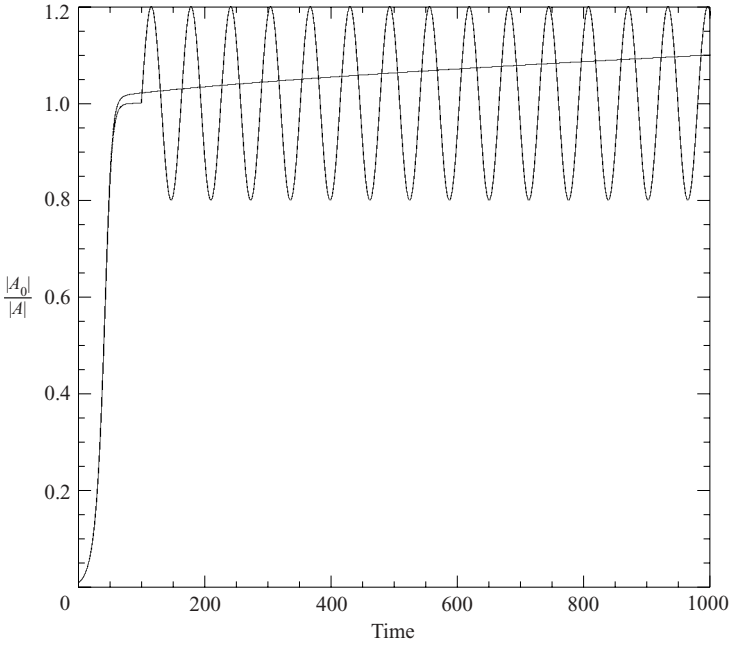

FIGURE 7. The two classes of model for the amplitude R used in calculating the particle dispersion: the first class, corresponding to inviscid critical layers, shows initial exponential growth followed by saturation to $R \sim 1$ and oscillatory behaviour; the second class, corresponding to the viscous case, follows the exponential phase with algebraic growth. We show only the oscillatory case with period 65; the shorter-period (6) case looks identical but for the period of the oscillation, but cannot be easily displayed on the same time plot for reasons of graphical clarity.

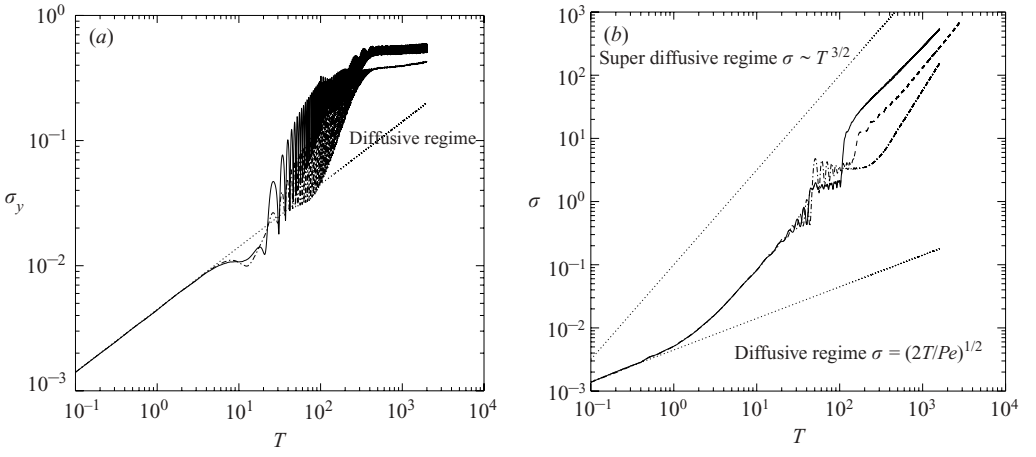

FIGURE 8. Results of our particle dispersion calculations, for the three amplitude models shown in the previous figure; in each panel, the solid line corresponds to the oscillatory case with period 6; the long dashed line to the oscillatory case with period 65; and the dash-dotted line to the viscous case, with ultimately algebraic amplitude growth. We show the particle dispersion σ in (a) the transverse direction and (b) the longitudinal direction.

in our case (as opposed to the Poiseuille case) the flow amplitude continues to show temporal variations in the long-time limit.

These results are consistent with anomalous diffusion found in other two-dimensional flows by Venkataramani, Antonsen & Ott (1998) that predict the $\sigma \sim T^{3/2}$ scaling for flows with KAM regions. The temporal periodicity in the flow in our first two cases creates the possibility for KAM regions to coexist with chaotic regions; and particle dispersion is in good agreement with theory. However, for the third case, the amplitude of the flow grows indefinitely with time, with no periodicity, and there do not exist any KAM regions; thus the absence of KAM regions (where particles can become trapped) and the indefinite growth of the vortices leads to particle transport that is more super-diffusive.

From the above particle simulation results, we expect that, despite the fact that the particle diffusion coefficient is the same, more diffusive particle dispersion can be found in viscous critical layers (third case in figure 8) than inviscid critical layers (first and second cases in figure 8). For the case of viscous critical layers, the single-wave asymptotic expansion eventually fails as the critical layer expands indefinitely. Thus it would be interesting to see how the mixing pattern might be altered when the critical layer comes in contact with the interface. In the case where multiple critical layers interact with each other, the ensuing mixing patterns are found to depend sensitively on various dimensionless parameters (Balmforth & Young 2002). In the present case of wind-driven gravity waves, the expanding viscous critical layer may cause the surface wave to break as the critical layer expands towards the interface, leading to complicated mixing, as observed in figure 9 below from direct numerical simulations of wind-driven gravity waves (Alexakis *et al.* 2004).

7. Discussion and conclusion

In this paper, we have conducted a weakly nonlinear analysis of the resonant interaction between wind and surface gravity waves based on our earlier linear analysis (Alexakis *et al.* 2002).

Our results indicate that the exponential growth of unstable resonant waves during the linear regime transitions to algebraic growth in the weakly nonlinear regime. For the parameters we have used to simulate the amplitude equations, the transition occurs when the surface amplitude $H \sim 60$, which translates to $h/l \sim 60\mathrm{e}^{-3\mathscr{A}_1 G}$ for the large G case, or $h/l \sim 60r^2$ for the small-density-ratio case. As pointed out by Reutov (1980), such a transition amplitude is extremely small for the air–water case as $r = 10^{-3}$ and $h/l \sim 6 \times 10^{-5}$. In the weakly nonlinear regime, the algebraic growth scales as $t^{2/3}$ with a prefactor linearly proportional to the weak viscosity in the critical layer, similar to cases without coupling with gravity waves.

We have also obtained an interesting result related to mixing at the 'saddle points' connecting neighbouring cat's eyes inside the critical layer; this mixing (which we studied by means of inserting Lagrangian tracers, and observing their evolution) is a consequence of the dynamics near the 'saddle', where mixing between two adjacent vortices appears to take place (see earlier related work by del Castillo-Negrete & Morrison 1993). Such mixing regions are commonly found in non-integrable Hamiltonian systems, and here they suggest the presence of chaotic mixing. Results from the particle analysis further confirm that chaotic mixing is a consequence of the temporal behaviour of the amplitude associated with the global background flow. Even though we have assumed much simpler temporal behaviour for the amplitude in our simulations, the super-diffusion found in the simpler cases affirms that more

chaotic mixing should be expected as a result of the instability of the shear flow coupled to the gravity surface waves. This may imply that the entrainment rate of water vapour into air could be enhanced by the coupling of weak wind with surface waves.

At the outset of our weakly nonlinear analysis we assume the spatial domain is periodic in the streamwise direction, and rely on the periodicity to avoid the problems of interaction between modes in the continuum without resorting to quasi-linear theory (Jenkins 1992) or eddy viscosity models (Belcher *et al.* 1994; Harris *et al.* 1996). Assuming that some dissipative and surface restoring force reduces the number of unstable modes to one, we focus on such a resonant mode inside the critical layer. The periodicity assumption, albeit unrealistic in most physical situations, is advantageous for comparison between our weakly nonlinear results and direct numerical simulations. The details of this process are elucidated in the following for various relevant physical scenarios where our results may be applicable.

The $G \equiv gl/U^2 \gg 1$ assumption can be relevant in astrophysics, where gravity is very large compared to convection 'winds' in the convection zone, or to the accretion flow on the white dwarf surface. However, there exists no capillary force in astrophysics. Magnetic fields aligned with the interface act similarly to the surface tension, yet the resultant dispersion relation is different; unlike surface tension the phase velocity of the waves does not increase with the wavenumber but instead saturates at the Alfvén speed. Therefore, contrary to the case with surface tension, modes with large wavenumbers are not neutralized or damped completely by magnetic fields, but their growth rate decreases exponentially with wavenumber. Thus, in the case of a magnetized plasma, we would also need to further assume that the most unstable mode is much more 'dominant' than any other mode in the continuum in order to apply our results to astrophysics. In terrestrial situations, the condition $G \gg 1$ can be met in liquid interfaces for large length scale of the wind ($l \gg U^2/g$) provided that the constraint $4\mathscr{T}G < (r+1)^2/(1-r)$ for instability is satisfied. For the small-density-ratio case ($r \ll 1$), the periodicity assumption and the criterion for surface tension to damp all the modes except the most unstable mode result in a range of the maximum wind velocity within which our weakly nonlinear results apply to small-density-ratio cases: $0.2\ \mathrm{m\,s^{-1}} < U_{max} < 1\ \mathrm{m\,s^{-1}}$ for the air–water case.

The calculations presented here provide useful information for validating numerical simulations of wind-driven interface instabilities. For cases of $G \gg 1$ or $r \ll 1$ the linear behaviour can be found only for amplitudes too small to be observed numerically; thus it will be challenging to verify linear theory. In contrast, it should be relatively easy to test the numerics in the weakly nonlinear limit.

We further remark that, as found in the case of an internal boundary layer (Balmforth & Young 2002), a similar nonlinear development of the vorticity in the critical layer and its ensuing expansion are also observed in direct numerical simulations with parameters well beyond the range suitable for weakly nonlinear analysis. Figure 9 illustrates such an example obtained from direct numerical simulation of wind-driven gravity waves with $G = 0.1$ and $r = 0.1$, no surface tension, and an initial maximum Mach number of $U_{max}/C_{sound} = 0.2$ (Alexakis *et al.* 2004). We note that while the characteristic parameters are beyond the range for weakly nonlinear analysis, the fully nonlinear results bear a strong similarity to the weakly nonlinear results discussed earlier. Thus, the cat's eye vorticity shown in figure 3 resembles the contour of scalar density field in figure 9(*a*), even though the vorticity has already expanded just above the interface. The temporal evolution of the wave energy is shown in figure 9(*b*). Despite the fast oscillations due to sound waves emitting

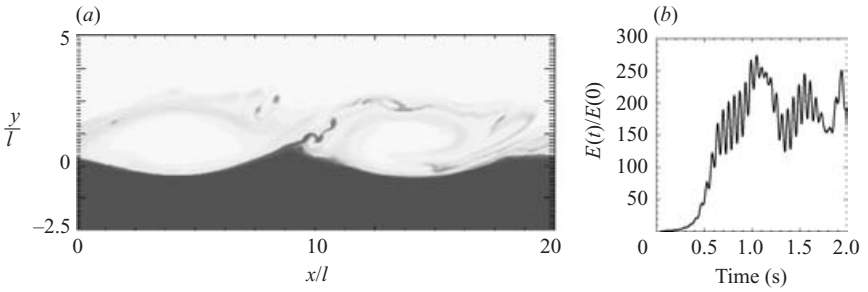

FIGURE 9. Results from direct numerical simulations with $G = 0.1$ and $r = 0.1$, obtained at a (dimensional) time of ~ 1 s. (*a*) Density contour plot of a wind-driven gravity wave; (*b*) the energy of the wave as a function of time.

from the reflecting bottom boundary, the temporal variation behaves similarly to the amplitude H for the weakly nonlinear case shown in figure 2 if the fast sound wave oscillations are filtered. Here it is especially notable that while the temporal evolution in these two rather different cases bears a remarkable resemblance, the physics underlying the saturation in these two cases is quite different: contrary to the weakly nonlinear case, the saturation in the fully nonlinear calculations results from the fact that the critical layer both broadens substantially and descends onto the interface (figure 9*a*); this behaviour strongly suggests that in this nonlinear regime, saturation is largely a consequence of the broadening of the resonant layer, and consequent decreased coupling between the wind and the perturbed interface. Thus, we see that the saturation mechanism is likely to depend on details of the specific parameter regime governing the shear layer; this is an issue we intend to pursue in much more detail in subsequent studies.

Finally, we note a number of interesting additional issues that remain to be investigated. For example, while we have focused on mixing above the interface, mixing below the interface can also have important astrophysical consequences; this is principally because (for example) mixing H and He into C/O of the white dwarf star can lead to nuclear burning in the upper layers of the star itself, which may significantly affect the stratification of the interface layer (because then the dynamics of the latter layer may resemble much more closely what occurs in atmospheres heated from below (e.g. the solar photospheric case). Similarly, subsurface currents (possibly due to subsurface convection) can also significantly couple to the interface instability (Cheung & Street 1988; Simmen & Saffman 1985; Saffman & Yuen 1982).

This work was supported in part by the DOE-funded ASCI/Alliances Center for Thermonuclear Flashes at the University of Chicago. We thank N. J. Balmforth, N. R. Lebovitz, and S. C. Venkataramani for helpful conversations. We would also like to thank the anonymous referees for pointing out additional crucial references and giving useful comments. Y. N. Y. acknowledges support from NASA and Northwestern University, and computation support from Argonne National Laboratory.

Appendix A. Large-G behaviour

We are interested in cases for which the factor G is large. As already discussed, such cases correspond not only to the astrophysical limit of strong surface stratification, but also to cases for which the wind is weak enough so that the growth rate of

(linearly) unstable modes is small, i.e. to cases for which our analysis is actually appropriate.

In order to proceed, we need to adopt a specific wind profile; in what follows, we will use a profile of the form $U=(1-\mathrm{e}^{-y})$. However, we note that our basic results hold for more general wind profiles. From equation (3.6) we know that the unstable modes will have K of the same order as G, and therefore $K\gg 1$; this allows us to write a WKBJ expansion for the solution of the perturbation stream function of equation (3.1) for the wind. The equation we have to solve for large K is therefore

$$\phi_{,yy}-\left[K^2+\frac{U_{,yy}}{U-C}\right]\phi=0. \tag{A 1}$$

The boundary condition at the interface is

$$KC^2-r[C^2\phi_y|_0-CU'|_0]-G(1-r)=0. \tag{A 2}$$

The WKBJ approximation will break down at two points: the first one is at $y=y_c$, where the critical layer is located; the second one is at $y=y_a$, where y_a is the solution of $K^2(U-C)+U_{,yy}=0$ and the second term in (A 1) becomes zero. For this reason, we will have to decompose the y-axis into three regions: (I). $0<y<y_c$; (II). $y_c<y<y_a$; (III). $y_a<y$. The first-order solutions of the WKBJ equations therefore are

$$\text{(I)}\qquad \phi=A_1\frac{1}{\sqrt{w}}\exp\left(-\int_0^y w\,\mathrm{d}y'\right)+B_1\frac{1}{\sqrt{w}}\exp\left(+\int_0^y w\,\mathrm{d}y'\right), \tag{A 3}$$

$$\text{(II)}\qquad \phi=A_2\frac{1}{\sqrt{w}}\sin\left(\int_{y_c}^y w\,\mathrm{d}y'-\pi/4\right)+B_2\frac{1}{\sqrt{w}}\cos\left(\int_{y_c}^y w\,\mathrm{d}y'-\pi/4\right), \tag{A 4}$$

$$\text{(III)}\qquad \phi=A_3\frac{1}{\sqrt{w}}\exp\left(-\int_{y_a}^y w\,\mathrm{d}y'\right), \tag{A 5}$$

where

$$w(y)=\sqrt{\left|K^2+\frac{U_{,yy}}{U-C}\right|}=\sqrt{\left|K^2-\frac{\mathrm{e}^{-y}}{1-C-\mathrm{e}^{-y}}\right|}, \tag{A 6}$$

and the $-\pi/4$ factor appearing in the solution for region (II) is inserted for convenience, to be exploited shortly. The coefficients A_1, B_1, A_2, B_2, A_3 are connected through the solutions at the points where the WKBJ approximation breaks down, and can be obtained using matched asymptotics. Thus, close to $y=y_a$ it is well-known that the solution is an Airy function (Olver 1997). Matching the two solutions we obtain that, for $y_c<y<y_a$,

$$\phi=\frac{2A_3}{\sqrt{w}}\left\{\sin[I_1]\cos\left[\int_{y_c}^y w\,\mathrm{d}y'-\pi/4\right]-\cos[I_1]\sin\left[\int_{y_c}^y w\,\mathrm{d}y'-\pi/4\right]\right\}, \tag{A 7}$$

and therefore

$$B_2=2A_3\sin[I_1],\quad A_2=-2A_3\cos[I_1], \tag{A 8}$$

where $I_1=\int_{y_c}^{y_a} w\,\mathrm{d}y'$. The solutions near the critical point $y=y_c$ satisfy the equation

$$\phi_{,yy}-\frac{U_c''}{U_c'y}\phi=0 \tag{A 9}$$

where $U_c''=U''|_{y=y_c}$ and $U_c'=U'|_{y=y_c}$. The solutions of the above equations are given in terms of $z=-(y-y_c)U_c''/U_c'>0$ by

$$f_1(z)=\sqrt{z}J_1(2\sqrt{z}),\quad f_2(z)=\sqrt{z}N_1(2\sqrt{z}), \tag{A 10}$$

where J_1, N_1 are, respectively, the first Bessel and Neumann (Bessel of the second kind) functions. The first terms in the asymptotic expansion for $y \to +\infty$ are

$$f_1(z) \simeq \frac{z^{1/4}}{\sqrt{\pi}}\sin\left(2z^{1/2} - \pi/4\right), \quad f_2(z) \simeq -\frac{z^{1/4}}{\sqrt{\pi}}\cos\left(2z^{1/2} - \pi/4\right). \tag{A 11}$$

Matching with the outer solution, we have

$$\phi = \sqrt{\pi}A_2 f_1(z) - \sqrt{\pi}B_2 f_2(z).$$

The asymptotic expansion for $z \to 0^+$ is

$$f_1 \simeq z + \cdots, \tag{A 12}$$

$$\pi f_2 \simeq -1 + z\ln|z| + \cdots - (1-2\gamma)z + \cdots, \tag{A 13}$$

where γ is the Euler–Masceroni constant. Thus, we can identify f_1 with the regular Frobenius solution ϕ_a, and f_2 with the singular Frobenius solution ϕ_b. Here we assumed that C_i is much smaller that G^{-1} (this is something that will be justified *a posteriori*).

For $y < y_c$ the solutions of equation (A 9) can be obtained by making the transformation $z \to \mathrm{e}^{-\mathrm{i}\pi}z$ which is equivalent to taking the contour below the critical layer. By doing this the first Bessel function transforms to the first modified Bessel function that is growing exponentially and is real while the second one transforms to a linear combination of an exponentially growing and an exponentially decreasing modified Bessel function, and due to the presence of the logarithm it will have an imaginary part. Their asymptotic expansion for $y \to \infty$ is

$$f_1 \simeq -\frac{z^{1/4}}{2\sqrt{\pi}}\mathrm{e}^{+2\sqrt{z}}, \quad f_2 \simeq \frac{z^{1/4}}{2\sqrt{\pi}}[\mathrm{i}\mathrm{e}^{2\sqrt{z}} - 2\mathrm{e}^{-2\sqrt{z}}], \tag{A 14}$$

with $z = (y - y_c)U_c''/U_c' > 0$. The inner solution for negative large z can be then written as

$$\phi_{in} \simeq \sqrt{\pi}(A_2 f_1 - B_2 f_2), \tag{A 15}$$

$$\simeq -\frac{z^{1/4}}{2}[(A_2 + \mathrm{i}B_2)\mathrm{e}^{2\sqrt{z}} - 2B_2\mathrm{e}^{-2\sqrt{z}}]. \tag{A 16}$$

Matching with the outer solution then gives

$$\phi \simeq \frac{1}{2\sqrt{w}}\left[-(A_2 + \mathrm{i}B_2)\exp\left(-\int_{y_c}^{y} w\,\mathrm{d}y'\right) + 2B_2\exp\left(+\int_{y_c}^{y} w\,\mathrm{d}y'\right)\right] \tag{A 17}$$

or

$$\phi = -\frac{A_2 + \mathrm{i}B_2}{2}\mathrm{e}^{I_2}\frac{1}{\sqrt{w}}\exp\left(-\int_0^y w\,\mathrm{d}y'\right) + B_2\mathrm{e}{-I_2}\frac{1}{\sqrt{w}}\exp\left(\int_0^y w\,\mathrm{d}y'\right), \tag{A 18}$$

where $I_2 = \int_0^{y_c} w\,\mathrm{d}y'$. Gathering all the terms then gives

$$A_1 = A_3(\cos[I_1] - \mathrm{i}\sin[I_1])\mathrm{e}^{+I_2}, \quad B_1 = 2A_3\sin[I_1]\,\mathrm{e}^{-I_2}, \tag{A 19}$$

and

$$\phi = A_3 \left[2\sin(I_1)\mathrm{e}^{-I_2} \exp\left(+ \int_0^y w \, \mathrm{d}y' \right) + \cos(I_1)\mathrm{e}^{+I_2} \exp\left(- \int_0^y w \, \mathrm{d}y' \right) - \mathrm{i}\sin(I_1)\mathrm{e}^{+I_2} \exp\left(+ \int_0^y w \, \mathrm{d}y' \right) \right]. \quad \text{(A 20)}$$

The values of ϕ and $\phi_{,y}$ at zero are therefore

$$\phi|_0 = A_3 \left[2\sin(I_1)\mathrm{e}^{-I_2} + \cos(I_1)\mathrm{e}^{+I_2} - i\sin(I_1)\mathrm{e}^{+I_2} \right], \quad \text{(A 21)}$$

$$\phi_{,y}|_0 = A_3 \left[2\sin(I_1)\mathrm{e}^{-I_2} - \cos(I_1)\mathrm{e}^{+I_2} + i\sin(I_1)\mathrm{e}^{+I_2} \right], \quad \text{(A 22)}$$

where we have kept terms only to first order in K. For the given wind profile $(1-\mathrm{e}^{-x})$, we have

$$y_c = -K\ln(1-C), \quad y_a = -[K\ln(1-C) - K\ln(1+1/K^2),$$

$$I_1 \simeq \frac{\pi}{2K} + O(1/K^3), \quad \text{(A 23)}$$

$$I_2 \simeq K y_c + O(1/K^2) = -K\ln(1-C) + O(1/K), \quad \text{(A 24)}$$

$$\sin(I_1) \simeq \frac{\pi}{2K}, \quad \cos(I_1) \simeq 1, \quad \mathrm{e}^{-I_2} = (1-C)^K.$$

Normalizing so that $\phi|_0 = 1$, we then obtain

$$\phi_{,y} = \frac{2\sin(I_1)\mathrm{e}^{-I_2} - \cos(I_1)\mathrm{e}^{+I_2} + \mathrm{i}\sin(I_1)\mathrm{e}^{+I_2}}{2\sin(I_1)\mathrm{e}^{-I_2} + \cos(I_1)\mathrm{e}^{+I_2} - \mathrm{i}\sin(I_1)\mathrm{e}^{+I_2}}, \quad \text{(A 25)}$$

or

$$\phi_{,y} = -1 + \frac{4\sin(I_1)\mathrm{e}^{-I_2}}{2\sin(I_1)\mathrm{e}^{-I_2} + \cos(I_1)\mathrm{e}^{+I_2} - \mathrm{i}\sin(I_1)\mathrm{e}^{+I_2}}. \quad \text{(A 26)}$$

The second term in equation (A 26) is exponentially small when compared to 1 since $I_2 \sim K$; neglecting this term when appropriate then allows $\phi_{,y}$ to be written as

$$\phi_{,y} = -1 + 4\mathrm{i}\sin^2(I_1)\mathrm{e}^{-2I_2}, \quad \text{(A 27)}$$

where we have kept only the first term in the expansion of the real and imaginary parts. Substituting this value of $\phi_{,y}$ in equation (A 2), we obtain, to zeroth order,

$$C_0 = \sqrt{\frac{1-rG}{1+rK}} = \sqrt{\mathscr{A}_t G/K}, \quad \text{(A 28)}$$

which corresponds to the gravity wave in the absence of a wind; $\mathscr{A}_t$ is the Atwood number. For our purposes, this is as far as we need to go in analysing the real part of C.

We next turn to analysing the imaginary part of C. To obtain the first order in $\mathrm{Im}\{C\} = C_i \ll C_0$ we have

$$2K(1+r)C_0C_i - rKC_0^2(1+\phi_{,y}) = 0, \quad C_i = \frac{1}{2}\frac{r}{1+r}C_0(1+\phi_{,y}), \quad \text{(A 29)}$$

so that

$$C_i = \frac{2rC_0}{1-r}\sin^2(I_1)\mathrm{e}^{-2I_2}, \quad \text{(A 30)}$$

or

$$\mathrm{Im}\{C_1\} = \frac{r\pi^2}{2(1+r)}\frac{1}{\mathscr{A}_t^2 G^2}\left(\frac{\mathscr{A}_t G}{K}\right)^{5/2}\left[\left(1-\frac{1}{\sqrt{K/(\mathscr{A}_t G)}}\right)^{(K/\mathscr{A}_t G)}\right]^{2\mathscr{A}_t G}. \quad (A\,31)$$

We note that $(1-1/\sqrt{x})^{2x}$ is a bounded function that is smaller than 1 with $q_m = \max(\ln(1-1/\sqrt{x})^{2x}) \simeq -2.45\ldots$, and therefore C_i has a negative exponential dependence on G and the result in (3.11) follows. We note further that this exponential dependence should be independent of the wind profile, and in a more general case – for which $U(y)$ is the wind profile and $U^{-1}(c)$ is its inverse – the growth rate will be proportional to $C_i \sim \exp[-2KU^{-1}(c)]$; this can be re-written as $C_i \sim f(c(K))^{\mathscr{A}_t G}$, with $f(c) \equiv \exp[-2U^{-1}(C)/C]$ a bounded function and $C = C_0$. The interpretation of equation (A 30) is straightforward: it simply states that the growth rate is proportional to the negative exponential of the height of the critical layer, as measured in units of the wavelength.

Appendix B. Rescaling (5.1)–(5.4)

Before we begin investigating the amplitude equations we rescale our system so that we are left with a minimum number of free parameters. By letting $Z = U''/\sqrt{U'}\tilde{Z}$, $Y = \eta/\sqrt{U'}$, $T = \tau/(\sqrt{U'}k)$, $\xi = Kx$ and $\nu = \nu'/\sqrt{U'}$ we obtain the following equation to be solved:

$$\tilde{Z}_{,\tau} + \eta\tilde{Z}_{,\xi} - \tilde{\Psi}_{0,\xi}\tilde{Z}_{,\eta} - \nu'\tilde{Z}_{,\eta\eta} = \tilde{\Psi}_{0,\xi},$$

with

$$J = \frac{1}{2\pi}\int_{-\pi}^{+\pi}\int_{-\infty}^{+\infty} \mathrm{e}^{-\mathrm{i}\xi}\tilde{Z}\,\mathrm{d}\eta\,\mathrm{d}\xi.$$

By rescaling A to $|\mathscr{C}_2|^2/|\mathscr{D}_1|^2 A$, and H to $|\mathscr{C}_2|^2/|\mathscr{D}_1|H$, we can always scale our system so that $\mathscr{D}_1 = 1$ and $\mathscr{C}_2 = -1$. Finally, the coefficient $\mathscr{C}_1$ can always be set to zero by performing a Galilean transformation ($\tau \to \tau + \mathscr{C}_1\xi$) and shifting the critical layer by $Y \to Y - \mathscr{C}_1$. The last transformation corrects the position of the critical layer to order ϵ. We are left therefore with two independent parameters, $\mathscr{D}_2$ and ν, to investigate. The parameter $\mathscr{D}_2$ gives a measure of the coupling of the critical layer to the wave ($\mathscr{D}_2 = 0$ gives the evolution of a 'free' critical layer uncoupled from gravity waves).

REFERENCES

Akylas, T. R. 1982 A nonlinear theory for the generation of water waves by wind. *Stud. Appl. Maths* **67**, 1–24.

Alexakis, A., Calder, A. C., Dursi, L. J., Fryxell, B., Kane, O., Olson, K., Ricker, P., Rosner, R., Timmes, F. X. & Zingale, M. 2004 Numerical simulations of wind driven waves. In Preparation.

Alexakis, A., Young, Y. & Rosner, R. 2002 Shear instability of fluid interfaces: Stability analysis. *Phys. Rev.* E **65**, 026313.

Balmforth, N. & Piccolo, C. 2001 The onset of meandering in a barotropic jet. *J. Fluid Mech.* **449**, 85–114.

Balmforth, N. J. & Young, Y.-N. 2002 Stratified Kolmogorov flow. *J. Fluid Mech.* **450**, 131–167.

Belcher, S. E., Harris, J. A. & Street R. L. 1994 Linear dynamics of wind waves in coupled turbulent air-water flow. Part 1. Theory. *J. Fluid Mech.* **271**, 119–151.

Benney, D. & Bergeron Jr., R. F. 1969 A new class of nonlinear waves in parallel flows. *Stud. Appl. Maths* **48**, 181–204.

Benney, D. & Maslowe, S. 1975 The evolution in space and time of nonlinear waves in parallel shear flows. *Stud. Appl. Maths* **54**, 181–205.

Blennerhassett, P. J. 1980 On the generation of waves by wind. *Phil. Trans. R. Soc. Lond.* A **298**, 451–494.

Boffetta, G., Lacorata, G., Radaelli G. & Vulpiani, A. 2001 Detecting barriers to transport: a review of different techniques. *Physica* D **159**, 58–70.

Caponi, E. A., Caponi, M. Z., Saffman, P. G. & Yuen, H. C. 1992 A simple model for the effect of water shear on the generation of waves by wind. *Proc. Roy. Soc. Lond.* A **438**, 95–101.

del Castillo-Negrete, D. 2000 Self-consistent chaotic transport in fluids and plasmas. *Chaos* **10**, 75–88.

del Castillo-Negrete, D. & Morrison, P. 1993 Chaotic transport by Rossby waves in shear flow. *Phys. Fluids* **5**, 948–965.

Chandrasekhar, S. 1961 *Hydrodynamic and Hydromagnetic Stability*. Clarendon.

Cheung, T. K. & Street, R. L. 1988 The turbulent layer in the water at an air-water interface. *J. Fluid Mech.* **194**, 133–151.

Churilov, S. & Shukhman, I. 1987 Nonlinear stability of a stratified shear-flow – a viscous critical layer *J. Fluid Mech.* **180**, 1–20.

Churilov, S. & Shukhman, I. 1996 The nonlinear critical layer resulting from the spatial or temporal evolution of weakly unstable disturbances in shear flows. *J. Fluid Mech.* **318**, 189–221.

Drazin, P. 1970 Kelvin-Helmholtz instability of finite amplitude. *J. Fluid Mech.* **42**, 321–335.

Drazin, P. & Reid, W. 1981 *Hydrodynamic Stability*. Cambridge University Press.

Goldstein, M. & Hultgren, L. 1988 Nonlinear spatial evolution of an externally excited instability wave in a free shear layer. *J. Fluid Mech.* **197**, 295–330.

Haberman, R. 1972 Critical layers in parallel flows. *Stud. Appl. Maths* **51**, 139–161.

Harris, J. A., Belcher, S. E. & Street, R. L. 1996 Linear dynamics of wind waves in coupled turbulent air-water flow. Part 2. Numerical model. *J. Fluid Mech.* **308**, 219–254.

Jenkins, A. D. 1992 A quasi-linear eddy-viscosity model for the flux of energy and momentum to wind waves using conservation-law equations in a curvilinear coordinate system. *J. Phys. Oceanogr.* **22**, 843–858.

Latini, M. & Bernoff, A. 2001 Transient anomalous diffusion in Poiseuille flow. *J. Fluid Mech.* **441**, 399–411.

Lingevitch, J. F. & Bernoff, A. J. 1994 Advection of a passive scalar by a vortex couple in the small diffusion limit. *J. Fluid Mech.* **270**, 219–249.

Maslowe, S. A., Benney D. J. & Mahoney, D. J. 1994 Wave packet critical layers in shear flows. *Stud. Appl. Maths* **91**, 1–16.

Miles, J. 1957 On the generation of surface waves by shear flows. *J. Fluid Mech.* **3**, 185–204.

Miles, J. 1959*a* On the generation of surface waves by shear flows. Part 2. *J. Fluid Mech.* **6**, 568–582.

Miles, J. 1959*b* On the generation of surface waves by shear flows. Part 3. Kelvin-Helmholtz instability. *J. Fluid Mech.* **6**, 583–598.

Miles, J. 1962 On the generation of surface waves by shear flows. Part 4. *J. Fluid Mech.* **13**, 433–448.

Miles, J. 1967 On the generation of surface waves by shear flows. Part 5. *J. Fluid Mech.* **30**, 163–175.

Miles, J. 1999 Wind-to-wave energy transfer. In *Wind-over-wave Couplings: Perspective and Prospects* (ed. S. G. Sajjadi, N. H. Thomas & J. C. R. Hunt). Clarendon.

Ngan, K. & Shepherd, T. G. 1997 Chaotic mixing and transport in Rossby-wave critical layers. *J. Fluid Mech.* **334**, 315–351.

Oikawa, M., Chow, K. & Benney, D. J. 1987 The propagation of nonlinear wave packets in a shear flow with a free surface. *Stud. Appl. Maths* **76**, 69–92.

Olver, F. 1997 *Asymptotics and Special Functions*. A K Peters.

Onishchenko, I. N., Linetskii, A. R., Matsiborko, N. G., Shapiro, V. D., & Shevchenko, V. I. 1970 Concerning the nonlinear theory of the excitation of a monochromatic plasma wave by an electron beam. *Pis'ma v ZhETF.* **12**, 8, 407–411.

Reutov, V. P. 1980 The plasma-hydrodynamic analogy and the nonlinear stage of instability of wind waves. *Izv. Atmos. Ocean. Phys.* **16**, 12, 938–943.

Rosner, R., Alexakis, A., Young, Y., Truran, J. & Hillebrandt, H. 2001 On the C/O enrichment of nova ejecta. *Astrophys. J.* **562**, L177–L179.

Saffman, P. G. & Yuen, H. C. 1982 Finite amplitude interfacial waves in the presence of a current. *J. Fluid Mech.* **123**, 389–410.

Shukhman, I. & Churilov, S. 1997 The effect of slight stratification on the nonlinear spatial evolution of a weakly unstable wave in a free shear layer. *J. Fluid Mech.* **343**, 197–233.

Simmen, J. A. & Saffman, P. G. 1985 Steady deap-water waves on a linear shear current. *Stud. Appl. Maths* **73**, 35–57.

Venkataramani, C., Antonsen, M. & Ott, E. 1998 Anomolous diffusion in bounded temporally irregular flows. *Physica* D **112**, 412–440.

Warn, T. & Warn, H. 1978 The evolution of a nonlinear critical level. *Stud. Appl. Maths* **59**, 37–71.